AD-A134 376 A GENERALIZED COUPLE THEORY OF HYGROTHERMAL-ELASTICITY: 1/1
TRANSIENT EFFECTS..(U) LEHIGH UNIV BETHLEHEM PA INST OF
FRACTURE AND SOLID MECHANICS.. G C SIH ET AL. SEP 83
UNCLASSIFIED AMMRC-TR-83-56 DAAG46-82-K-0006 F/G 11/4 NL

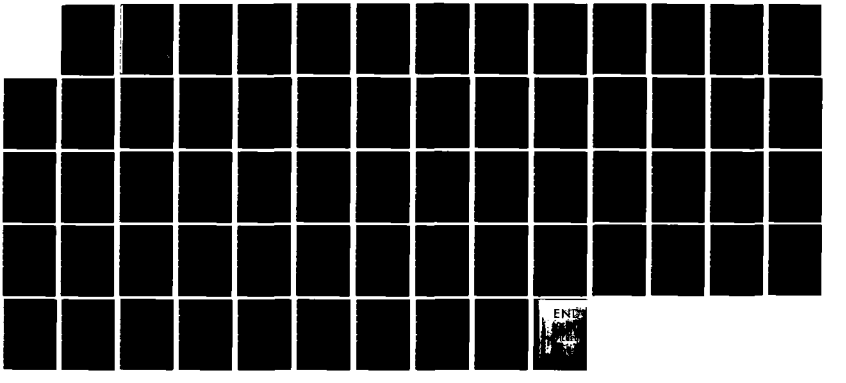

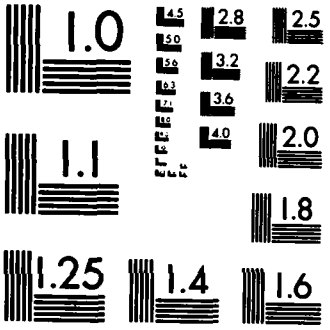

MICROCOPY RESOLUTION TEST CHART
NATIONAL BUREAU OF STANDARDS-1963-A

AMMRC TR 83-56

A GENERALIZED COUPLE THEORY OF HYGROTHERMAL-ELASTICITY: TRANSIENT EFFECTS IN COMPOSITE LAMINATE WITH CIRCULAR CAVITY

September 1983

G. C. SIH and M. T. SHIH
Institute of Fracture and Solid Mechanics
Lehigh University
Bethlehem, Pennsylvania 18015

FINAL REPORT

Contract No. DAAG46-82-K 0006

Prepared for

ARMY MATERIALS AND MECHANICS RESEARCH CENTER
Watertown, Massachusetts 02172

The findings in this report are not to be construed as an official Department of the Army position, unless so designated by other authorized documents.

Mention of any trade names or manufacturers in this report shall not be construed as advertising nor as an official indorsement or approval of such products or companies by the United States Government.

DISPOSITION INSTRUCTIONS

Destroy this report when it is no longer needed.
Do not return it to the originator.

UNCLASSIFIED

SECURITY CLASSIFICATION OF THIS PAGE (When Data Entered)

REPORT DOCUMENTATION PAGE	READ INSTRUCTIONS BEFORE COMPLETING FORM
1. REPORT NUMBER: AMMRC TR 83-56	2. GOVT ACCESSION NO.: A134376
3. RECIPIENT'S CATALOG NUMBER:	
4. TITLE (and Subtitle): A GENERALIZED COUPLE THEORY OF HYGROTHERMAL-ELASTICITY: TRANSIENT EFFECTS IN COMPOSITE LAMINATE WITH CIRCULAR CAVITY	5. TYPE OF REPORT & PERIOD COVERED: Final Report - 1 Nov 81 to 1 Jan 83
	6. PERFORMING ORG. REPORT NUMBER:
7. AUTHOR(s): G. C. Sih and M. T. Shih	8. CONTRACT OR GRANT NUMBER(s): DAAG46-82-K-0006
9. PERFORMING ORGANIZATION NAME AND ADDRESS: Institute of Fracture and Solid Mechanics, Lehigh University, Bethlehem, Pennsylvania 18015	10. PROGRAM ELEMENT, PROJECT, TASK AREA & WORK UNIT NUMBERS: D/A Project: 8H363304D215 AMCMS Code: 603000.2156
11. CONTROLLING OFFICE NAME AND ADDRESS: Army Materials and Mechanics Research Center, ATTN: DRXMR-K, Watertown, Massachusetts 02172	12. REPORT DATE: September 1983
	13. NUMBER OF PAGES: 51
14. MONITORING AGENCY NAME & ADDRESS (if different from Controlling Office)	15. SECURITY CLASS (of this report): Unclassified
	15a. DECLASSIFICATION/DOWNGRADING SCHEDULE

16. DISTRIBUTION STATEMENT (of this Report)

Approved for public release; distribution unlimited.

17. DISTRIBUTION STATEMENT (of the abstract entered in Block 20, if different from Report)

18. SUPPLEMENTARY NOTES

19. KEY WORDS (Continue on reverse side if necessary and identify by block number)

Hygrothermal effects	Temperature	Composite materials
Moisture content	Stress Analysis	Transient response
Elastic properties	Finite element analysis	Hydroelasticity

20. ABSTRACT (Continue on reverse side if necessary and identify by block number)

(SEE REVERSE SIDE)

DD FORM 1 JAN 73 1473 EDITION OF 1 NOV 65 IS OBSOLETE

UNCLASSIFIED

SECURITY CLASSIFICATION OF THIS PAGE (When Data Entered)

Block No. 20

ABSTRACT

A system of coupled differential equations involving moisture, temperature and stress are derived within the framework of classical thermodynamics. Analyzed are the transient character of the stress and energy density distribution around a circular cavity in a cross-ply graphite T300/5208 epoxy resin laminate assumed to behave in a quasi-isotropic manner. The laminate is stretched uniaxially such that the mutual interaction of moisture, temperature and stress depend on whether the laminate is in a state of plane strain or plane stress. Unlike the case of moisture-temperature and stress being uncoupled, the diffusion coefficients for plane strain must be distinguished from those for plane stress when stress coupling effects are included. Time-dependent numerical results are obtained from a finite element formulation and reveal that stress coupling can have a marked influence on the solution, both qualitatively and quantitatively. This is particularly significant near defects or cavities where the stress and energy state experience high elevation. The neglect of stress coupling can lead to unconservative predictions. Possible failure sites are predicted from the strain energy density criterion which assume that excessive dilatation is associated with material separation while excessive distortion with yielding. As the magnitude of the applied uniaxial stress is increased, the predicted failure site tends to move closer to the cavity boundary. The present theory and method of analysis provide a quantitative assessment of moisture, temperature and mechanical load effects on material failure.

Foreword

The work in this report is prepared for the Army Materials and Mechanics Research Center (AMMRC) under Contract No. DAAG46-82-K-0006 with the Institute of Fracture and Solid Mechanics at Lehigh University, Bethlehem, Pennsylvania. The authors are particularly grateful to the Project Manager, Mr. J. F. Dignam and Technical Monitor, Dr. S.-C. Chou from AMMRC. Their constant interest and encouragement have made the progress in this work possible.

A GENERALIZED COUPLE THEORY OF HYGROTHERMAL-ELASTICITY: TRANSIENT EFFECTS IN COMPOSITE LAMINATE WITH CIRCULAR CAVITY

by

G. C. Sih and M. T. Shih
Institute of Fracture and Solid Mechanics
Lehigh University
Bethlehem, Pennsylvania 18015

ABSTRACT

A system of coupled differential equations involving moisture, temperature and stress are derived within the framework of classical thermodynamics. Analyzed are the transient character of the stress and energy density distribution around a circular cavity in a cross-ply graphite T300/5208 epoxy resin laminate assumed to behave in a quasi-isotropic manner. The laminate is stretched uniaxially such that the mutual interaction of moisture, temperature and stress depend on whether the laminate is in a state of plane strain or plane stress. Unlike the case of moisture-temperature and stress being uncoupled, the diffusion coefficients for plane strain must be distinguished from those for plane stress when stress coupling effects are included. Time-dependent numerical results are obtained from a finite element formulation and reveal that stress coupling can have a marked influence on the solution, both qualitatively and quantitatively. This is particularly significant near defects or cavities where the stress and energy state experience high elevation. The neglect of stress coupling can lead to unconservative predictions. Possible failure sites are predicted from the strain energy density criterion which assume that excessive dilatation is associated with material separation while excessive distortion with yielding. As the magnitude of the applied uniaxial stress is increased, the predicted failure site tends to move closer to the cavity boundary. The present theory and method of

analysis provide a quantitative assessment of moisture, temperature and mechanical load effects on material failure.

INTRODUCTION

A critical aspect of composite materials is the influence of environments such as temperature and moisture in addition to mechanical loads on their life expectancy. Despite the numerous test data collected in the past, the degradation of composite stiffness and strength due to environment is still not understood and has not been appropriately quantified. Empirical approaches are not only costly but cannot lead to a fundamental understanding of coupling between mechanical deformation and diffusion. In the absence of this knowledge, composites cannot be successfully applied in design and manufacture.

In a series of papers [1-4], coupled diffusion theories involving moisture and temperature were derived on the basis of classical thermodynamics. Numerous examples were solved to show that uncoupling of moisture and temperature cannot be justified in general. Appreciable difference attributed to coupling can result when the surface temperature is changed suddenly. This alters the transient character of the moisture distribution that also affects the resulting stresses and/or strains. Loading type also interacts with the diffusion process in a complex fashion. Because of the complexities of the theoretical treatment and procedures involved in determining the physical constants, only a few cases have been analyzed up to this date.

A recent experiment [5] has shown that the applied stress can indeed significantly affect the moisture and temperature distribution in composite materials. Such findings are not unexpected and suggest the need to consider coupling between

mechanical deformation and diffusion by moisture and temperature. Such a theory leading to three simultaneous partial differential equations will be presented in this work. The method of analysis will involve an iteration procedure in which initial values of moisture and temperature will be assumed to calculate the corresponding stress state. The iteration is repeated many times until all governing equations and transient boundary conditions are satisfied. Results are obtained specifically for a T300/5208 graphite epoxy laminate with a circular hole stretched uniaxially while the surface moisture is changed suddenly at a constant surface temperature. The stresses near the hole are found to oscillate in time and to deviate significantly from the corresponding uncoupled* results for small time. In accordance with the strain energy density criterion [6,7], the uncoupled solution can underestimate the threshold of material damage due to fracture initiation.

A COUPLED THEORY OF HYGROTHERMAL ELASTICITY

Based on the classical thermodynamic argument, a coupled theory of mechanical deformation and diffusion involving moisture and temperature will be derived. The governing equations reduce to those treated earlier when deformation is uncoupled [1-4]. In the absence of moisture, the classical coupled equations of thermoelasticity are obtained.

Thermodynamic State. Let the state of a unit volume of a solid be described by the temperature T, moisture C, entropy S, chemical potential P, stress tensor $\underset{\sim}{\sigma}$ and strain tensor $\underset{\sim}{e}$. The initial state of the solid is assumed to be in thermodynamic equilibrium with the properties T_o, C_o, S_o, P_o and vanishing $\underset{\sim}{\sigma}$ and $\underset{\sim}{e}$.

*In this work, uncoupling refers only to the interdependence of mechanical deformation and diffusion. Moisture and temperature are assumed to be coupled.

For small deviations from the equilibrium state, a potential Φ may be expanded in a power series by neglecting those terms higher than the second order [8]:

$$\Phi = \Phi_o - S_o\Delta T + P_o\Delta C - \frac{1}{3}\sigma_{ii} - \frac{\rho c_p}{2T_o}\Delta T^2 + d_t\Delta T\Delta C + \frac{1}{2}d_c\Delta C^2$$

$$- \frac{1}{4G}\sigma_{ij}\sigma_{ij} - \beta\sigma_{ii}\Delta C - \alpha\sigma_{ii}\Delta T - \frac{1}{2}\left(\frac{1}{9k} - \frac{1}{6G}\right)\sigma_{ii}^2,\ i,j = 1,2,3 \qquad (1)$$

in which ρ is the mass density, c_p the specific heat capacity, α the linear thermal expansion coefficient, β the linear moisture expansion coefficient, G the shear modulus of elasticity and $k = E/3(1-2\nu_p)$ the bulk modulus of elasticity with E being the Young's modulus and ν_p the Poisson's ratio. In equation (1), the coefficient d_c and d_t are defined as

$$d_c = \left(\frac{\partial P}{\partial C}\right)_{\sigma_{ii},T},\ d_t = \left(\frac{\partial P}{\partial T}\right)_{\sigma_{ii},C} \qquad (2)$$

The chemical potential p is given by

$$P = \frac{\partial\Phi}{\partial C} = P_o + d_t\Delta T + d_c\Delta C - \beta\sigma_{ii} \qquad (3)$$

The entropy S and strain components e_{ij} are obtainable from the thermodynamic potential Φ according to

$$S = -\frac{\partial\Phi}{\partial T} = S_o + \frac{\rho c_p}{T_o}\Delta T - d_t\Delta C + \alpha\sigma_{ii} \qquad (4)$$

and

$$e_{ij} = -\frac{\partial \Phi}{\partial \sigma_{ij}} - \frac{1}{3}\delta_{ij} = \frac{1}{2G}\left(\sigma_{ij} - \frac{\nu_p}{1+\nu_p}\sigma_{kk}\delta_{ij}\right) + (\alpha\Delta T + \beta\Delta C)\delta_{ij} \tag{5}$$

The coupling of moisture, temperature and mechanical deformation is thus reflected in Φ as given in equation (1).

Conservation Laws. The conservation of mass and energy will be invoked to describe the diffusion and stress state in the solid at a given time t. Let $\underset{\sim}{f}$ be the flux of moisture per unit area and time, mass conservation requires that

$$\nabla \cdot \underset{\sim}{f} + \frac{\partial C}{\partial t} = 0 \tag{6}$$

Moreover, the conservation of energy leads to an expression for the rate of change of internal energy with time:

$$\frac{\partial U}{\partial t} = -\nabla \cdot \underset{\sim}{q} + \sigma_{ij}\frac{\partial e_{ij}}{\partial t} \tag{7}$$

in which $\underset{\sim}{q}$ stands for the heat flux vector and

$$\nabla \cdot \underset{\sim}{q} = -T\frac{\partial S}{\partial t} + \Delta P \frac{\partial C}{\partial t} \tag{8}$$

where $\Delta P = P - P_o$. Application of the Onsager principle [2,3] leads to the following expressions for the moisture and heat flux vectors

$$\begin{aligned} \underset{\sim}{f} &= L_{11}\underset{\sim}{x}_f + L_{12}\underset{\sim}{x}_q \\ \underset{\sim}{q} &= L_{21}\underset{\sim}{x}_f + L_{22}\underset{\sim}{x}_q \end{aligned} \tag{9}$$

with L_{ij} $(i,j = 1,2)$ being the Onsager coefficients such that

$$L_{11} > 0,\ L_{22} > 0,\ L_{12} = L_{21} < \sqrt{L_{11}L_{22}} \tag{10}$$

The vectors $\underset{\sim}{x}_f$ and $\underset{\sim}{x}_q$ are given by

$$\begin{aligned} \underset{\sim}{x}_f &= -\,T\nabla\left(\frac{P}{T}\right) \simeq (d_t\Delta T + d_c\Delta C - \beta\sigma_{ii})\,\frac{\Delta T}{T} - d_t\nabla T - d_c\nabla C + \beta\nabla\sigma_{ii} \\ \underset{\sim}{x}_q &= -\,\frac{1}{T}\,\nabla T \end{aligned} \tag{11}$$

Substituting equations (11) into (9) and making use of equation (6) yield

$$(L_{11}d_t + \frac{1}{T_o}L_{12})\nabla^2 T + L_{11}d_c\nabla^2 C - L_{11}\beta\nabla^2\sigma_{ii} = \frac{\partial C}{\partial t} \tag{12}$$

Similarly, combining equations (4), (8) and (9) renders the relation

$$\begin{aligned} (L_{21}d_t + \frac{1}{T_o}L_{22})\nabla^2 T + L_{21}d_c\nabla^2 C - L_{21}\beta\nabla^2\sigma_{ii} &= \rho c_p\,\frac{\partial T}{\partial t} - T_o d_t\,\frac{\partial C}{\partial t} \\ &+ T_o\alpha\,\frac{\partial\sigma_{ii}}{\partial t} \end{aligned} \tag{13}$$

In deriving equations (12) and (13), it was assumed that $|d_c\Delta C|$ and $|\beta\sigma_{ii}|$ are smaller in comparison with $|d_t T_o|$ and that $|\Delta T| \ll T_o$. The remaining coupled equation will be found from the theory of elasticity.

Equation of Motion. The equation of motion can be written as

$$\frac{\partial\sigma_{ij}}{\partial x_j} = \rho\,\frac{\partial^2 u_i}{\partial t^2} \tag{14}$$

where u_i are the components of the displacement vector $\underset{\sim}{u}$. From the linear theory of elasticity, the stress-strain relation is

$$\sigma_{ij} = 2G \left[e_{ij} + \frac{\nu_p}{1-2\nu_p} e_{kk}\delta_{ij} - \frac{1+\nu_p}{1-2\nu_p} (\alpha\Delta T + \beta\Delta C)\delta_{ij}\right] \tag{15}$$

where ν_p is the Poisson's ratio of the solid. Putting equation (15) into (14) and knowing

$$e_{ii} = \nabla \cdot \underset{\sim}{u} \tag{16}$$

it can be shown that

$$\frac{1}{c_2^2} \frac{1-\nu_p}{1+\nu_p} \frac{\partial^2\sigma_{ii}}{\partial t^2} + \frac{6G}{c_2^2} \frac{1-\nu_p}{1-2\nu_p} \left(\alpha \frac{\partial^2 T}{\partial t^2} + \beta \frac{\partial^2 C}{\partial t^2}\right) = \frac{1-\nu_p}{1+\nu_p} \nabla^2\sigma_{ii} + 4G(\alpha\nabla^2 T + \beta\nabla^2 C) \tag{17}$$

For a quasi-static process where the speed of diffusion and load application is much slower than the speed of shear wave velocity

$$c_2 = \sqrt{\left(\frac{1-\nu_p}{1-2\nu_p}\right) \frac{2G}{\rho}} \tag{18}$$

equation (17) may be simplified as

$$\frac{1-\nu_p}{2E} \nabla^2\sigma_{ii} + \alpha\nabla^2 T + \beta\nabla^2 C = 0 \tag{19}$$

Solving for σ_{ii} from equation (19), it is obvious that

$$\sigma_{ii} = -\frac{2E}{1-\nu_p} [\alpha\Delta T + \beta\Delta C] + \phi \tag{20}$$

in which the Laplacian of ϕ vanishes, i.e.,

$$\nabla^2\phi = 0 \tag{21}$$

It is seen that equations (12), (13) and (19) are the system of governing equations solving for T, C and σ_{ii}.

Coupled Equations. The system of equations derived earlier can be rearranged into forms that are more recognizable when compared to the corresponding equations in the uncoupled theories. Eliminating σ_{ii} in equations (12) and (13) by applying equation (20), the following coupled equations are found:

$$\begin{aligned} D\nabla^2 C &= \frac{\partial C}{\partial t} - \lambda \frac{\partial R}{\partial t} \\ \mathcal{D}\nabla^2 R &= \frac{\partial R}{\partial t} - \nu \frac{\partial C}{\partial t} \\ \nabla^2\phi &= 0 \end{aligned} \tag{22}$$

in which

$$R = T + N\phi \tag{23}$$

Note that there are five physical constants D, $\mathcal{D}$, λ, ν and N in this theory. They are interconnected through the parameters L_{ij} (i,j = 1,2), d_c, d_t, etc., as follows:

$$\begin{aligned} D &= (1-\lambda\nu)D_m \\ \mathcal{D} &= (1-\lambda\nu)D_h \end{aligned} \tag{24}$$

in which D_m and D_h are given by

$$D_m = \left(\frac{2E\beta^2}{1-\nu_p} + d_c\right)L_{11}$$

$$D_h = \left(AT_oL_{11} + \frac{1}{T_o}L_{22} + 2L_{12}AT_o\right)/\left(\frac{\rho c_p}{T_o} - \frac{2E\alpha^2}{1-\nu_p}\right) \tag{25}$$

The quantity A stands for

$$A = \frac{2E\alpha\beta}{1-\nu_p} + d_t \tag{26}$$

The remaining constants in equations (22) and (23) are

$$\lambda = \left(AL_{11} + \frac{1}{T_o}L_{12}\right)\left(\frac{\rho c_p}{T_o} - \frac{2E\alpha^2}{1-\nu_p}\right)/\left(AT_oL_{11} + \frac{1}{T_o}L_{22} + 2L_{12}AT_o\right)$$

$$\nu = \left(\frac{1}{T_o}\frac{L_{21}}{L_{11}} + A\right)/\left(\frac{\rho c_p}{T_o} - \frac{2E\alpha^2}{1-\nu_p}\right) \tag{27}$$

$$N = \alpha/\left(\frac{\rho c_p}{T_o} - \frac{2E\alpha^2}{1-\nu_p}\right)$$

This completes the formulation of the coupled theory of hygrothermal elasticity.

PLANE THEORIES OF HYGROTHERMAL ELASTICITY AND SPECIAL CASES

When a length dimension of the solid, say in the z-direction, is either very small or large in comparison with the planar dimensions in the xy domain, certain approximations on the governing equations can be made. This will not only alter the form of the equations but also the definitions of the physical constants. The two cases that will be discussed are plane stress and plane strain state as defined in the classical theory of elasticity.

Plane Stress. For thin plates with surfaces free from tractions, the transverse normal stress component σ_{33} may be assumed to vanish and σ_{ii} equals to $\sigma_{11}+\sigma_{22}$ in equations (12) and (13). Since it is easier to perform experiments on thin plates, the physical constants D, $\mathcal{D}$, D_m, D_h, etc., in equations (24) through (27) shall refer to the case of plane stress.

Plane Strain. For long cylindrical bodies with axes along the z-direction, the longitudinal strain components may be assumed to vanish, i.e., $e_{33} = 0$. Making use of equation (15) with $e_{33} = 0$, it is found that

$$\sigma_{33} = \nu_p(\sigma_{11}+\sigma_{22}) - E[\alpha\Delta T + \beta\Delta C] \tag{28}$$

Substituting equation (28) into (15) gives

$$e_{ij} = \frac{1+\nu_p^*}{E^*}\left(\sigma_{ij} - \frac{\nu_p^*}{1+\nu_p^*}\sigma_{kk}\delta_{ij}\right) + \alpha^*\Delta T + \beta^*\Delta C \tag{29}$$

Here, $\sigma_{kk} = \sigma_{11}+\sigma_{22}$. Equations (29) and (15) are equivalent if

$$\alpha^* = (1+\nu_p)\alpha, \quad \beta^* = (1+\nu_p)\beta$$
$$\nu_p^* = \frac{\nu_p}{1-\nu_p}, \quad E^* = \frac{E}{1-\nu_p^2} \tag{30}$$

Henceforth, those quantities referred to the plane strain state will be distinguished by attaching an asterisk to them:

$$c_p^* = c_p - \frac{E}{\rho}\alpha^2$$

$$d_t^* = d_t + \frac{E}{\rho}\alpha\beta \tag{31}$$

$$d_c^* = d_c + \frac{E}{\rho}\beta^2$$

Thus, the same governing equations apply to plane stress and plane strain. Only the constants need to be replaced as indicated in equations (30) and (31).

Uncoupled Deformation. When the mechanical deformation term $N\phi$ in equation (23) is neglected, equations (22) reduce to

$$D\nabla^2 C = \frac{\partial C}{\partial t} - \lambda \frac{\partial T}{\partial t}$$

$$\mathcal{D}\nabla^2 T = \frac{\partial T}{\partial t} - \nu \frac{\partial C}{\partial t} \tag{32}$$

which have already been discussed previously [2].

Thermoelasticity Theory. By dropping those terms in equations (12), (13) and (15) pertaining to moisture change, the coupled thermoelastic equations may be obtained:

$$\rho c_p \frac{\partial T}{\partial t} + \alpha T_o \frac{\partial \sigma_{ii}}{\partial t} = (d_t L_{21} + \frac{1}{T_o} L_{22})\nabla^2 T$$

$$\sigma_{ij} = 2G\left[e_{ij} + \frac{\nu_p}{1-2\nu_p} e_{kk}\delta_{ij} - \frac{1+\nu_p}{1-2\nu_p}\alpha\Delta T\delta_{ij}\right] \tag{33}$$

The coefficients in equations (33) may be redefined to coincide with those given in the text book.

DETERMINATION OF PHYSICAL CONSTANTS

One of the major tasks of evaluating the coupling effects of moisture, temperature and mechanical deformation is a knowledge of the physical constants. The material depicted will be that of a T300/5208 graphite epoxy composite laminate which will be assumed to behave as a quasi-isotropic solid. The coupled theory solution will be obtained for the case where the coupling effects are weak such that the results can be compared with the uncoupled experimental data to extract the coupling constants.

Rule of Mixture. The rule of mixture will be first applied to obtain an average value of the thermal expansion coefficient α for the composite with 56% fiber volume fraction V_f. Let α_m and α_f denote the respective values of the thermal expansion coefficient for the matrix and fiber. The value α for the composite may be estimated from [10]

$$\log\alpha = V_m \log\alpha_m + V_f \log\alpha_f \tag{34}$$

or [11]

$$\alpha = \alpha_m \left[1 - V_f\left(1 - \frac{\alpha_f}{\alpha_m}\right)M\right] \tag{35}$$

in which M is given by

$$M = \frac{3(E_f/E_m)(1-V_m)}{[2V_f(1-2V_m)+(1+V_m)](E_f/E_m)+2(1-2V_f)(1-V_f)} \tag{36}$$

The Young's moduli of fiber and matrix are denoted by E_f and E_m, respectively.

The composite modulus in the direction of fiber reinforcement may be approximated by

$$E_{11} = E_f V_f + E_m V_m \tag{37}$$

The modulus in the transverse direction will be denoted by E_{22}. An approximate value E for a laminate with cross-plies can be written as [12]

$$E = \frac{3}{8} E_{11} + \frac{5}{8} E_{22} = 67.155 \text{ GPa} \tag{38}$$

Based on these assumptions, the quasi-isotropic properties of the T300/5208 graphite epoxy composite laminate are given in Table 1.

Table 1 - Material properties for T300/5208 graphite epoxy composite laminate [13]

	Graphite Fiber	Epoxy Matrix	Composite Laminate
Axial Modulus E_{11}(GPa)	276.00	E_m = 3.51-0.003T - 0.142C	156.08
Transverse Modulus E_{22}(GPa)	13.8	E_m = 3.51-0.003T - 0.142C	13.80
Poisson's Axial Ratio $(\nu_p)_{11}$	0.20	0.33	0.33
Poisson's Transverse Ratio $(\nu_p)_{22}$	0.25	0.33	
Axial Thermal Coefficient α_{11}/°C	-1.8×10^{-6}	45.0×10^{-6}	31.3×10^{-6}
Transverse Thermal Coefficient α_{22}/°C	21.6×10^{-6}	45.0×10^{-6}	
Moisture Coefficient β/wt%H_2O	0	2.68×10^{-3}	2.68×10^{-3}

The specific heat c_p of the T300/5208 laminate can be estimated from those for the matrix, water and fiber. They are given by

$$(c_p)_m = 0.22 \text{ cal/g°C}, \quad (c_p)_{H_2O} = 0.99 \text{ cal/g°C}$$

$$(c_p)_f = 0.336 + 9.50 \times 10^{-5} T - 1.70 \times 10^4 \frac{1}{T^2} \tag{39}$$

$$= 0.167 \text{ cal/g°C} \quad \text{at } T = 294°K$$

It is also known from [14] that the weight of one cubic meter of T300/5208 composite is 1,590 Kg and 1,608.48 Kg after fully saturated by moisture. This yields a difference of 18.48 Kg. Since the fiber weight percentage is 73.5, the fiber weight percentage corresponding to the fully saturated state may be computed as

$$(\% \text{ wt})_f = \frac{1,590}{1,608.48} (73.5\%) = 72.7\% \tag{40}$$

Under these considerations, a value of c_p for the laminate is obtained:

$$c_p = (\% \text{ wt})_f (c_p)_f + (\% \text{ wt})_m (c_p)_m + (\% \text{ wt})_{H_2O} (c_p)_{H_2O}$$

$$= (0.727)(0.167) + (0.262)(0.220) + (0.012)(0.99)$$

$$= 0.19041 \text{ cal/g°C} \tag{41}$$

Unit Conversion. Before deriving the physical constants in equations (22) and (23), it is necessary to make use of the results in [3,4] which refer to C as mass of moisture per unit volume of void. The corresponding constants D_v, $\mathcal{D}_v$ and $\lambda_v \nu_v$

for the T300/5208 material are given by

$$\frac{D_v}{\mathcal{D}_v} = 0.1, \quad \lambda_v \nu_v = 0.25 \tag{42}$$

The quantities D, $\mathcal{D}$, and $\lambda\nu$ in equations (22) correspond to C expressed as mass of moisture per unit volume of solid. The relationships

$$D = \frac{D_v}{1 + \frac{D_v}{\mathcal{D}_v} \lambda_v \nu_v}, \quad \mathcal{D} = \frac{\mathcal{D}_v}{1-\lambda_v \nu_v} \tag{43}$$

$$\lambda\nu = \frac{\lambda_v \nu_v}{1 + \frac{D_v}{\mathcal{D}_v} \lambda_v \nu_v} \frac{D_v}{\mathcal{D}_v}$$

given in [2] may be used for the conversion. From equations (42) and (43), it is found that

$$\frac{D}{\mathcal{D}} = 0.07317, \quad \lambda\nu = 0.02439 \tag{44}$$

The individual values of D, $\mathcal{D}$, λ and ν may be obtained by applying equations (24) and the relations

$$\lambda = \frac{D_m}{D_h} \frac{C_o Q_o}{R_g T_o^2}, \quad \nu = \frac{Q_o}{\rho c_p} \tag{45}$$

in which ρ is the mass density, R_g the gas constant, C_o the weight of moisture absorbed by one cubic meter of the composite at 21°C and 75% RH, Q_o is a constant, T_o = 294°K, and c_p is given by equation (41).

Coupled Constants for Plane Stress. It was pointed out in [2] that the diffusion coefficients for sudden moisture change D_m^c and D_h^c should be distinguished from D_m^T and D_h^T corresponding to sudden temperature change. These quantities are expressible in terms of D, $\mathcal{D}$, λ and ν as follows*:

$$D_m^c = \frac{1-\lambda\nu f(u,\lambda\nu)}{1-\lambda\nu} D$$

$$D_h^c = \frac{f(1/u,\lambda\nu)}{1-\lambda\nu} D \tag{46}$$

and

$$D_m^T = \frac{f(u,\lambda\nu)}{1-\lambda\nu} \mathcal{D}$$

$$D_h^T = \frac{1-\lambda\nu f(1/u,\lambda\nu)}{1-\lambda\nu} \mathcal{D} \tag{47}$$

in which the function $f(u,\lambda\nu)$ stands for

$$f(u,\lambda\nu) = [1 + u + \sqrt{4u(1-\lambda\nu)}]^{-1} = 0.62207 \tag{48}$$

since the numerical values of $u = D/\mathcal{D}$ and $\lambda\nu$ are known from equations (44). Knowing from [14] that

$$D_m^c = D_o \exp(E_o/R_g T_o) = 7.7954 \times 10^{-7} \text{ cm}^2/\text{hr} \tag{49}$$

*As discussed in [2], these constants can be measured experimentally by subjecting the specimen to sudden moisture or temperature change.

where E_o is the activation energy. The moisture diffusivity D_m^c in equation (49) for the T300/5208 material is calculated from the following constants:

$$D_o = 1.53 \times 10^3 \text{ cm}^2/\text{hr}, \; E_o = 1.25 \times 10^4 \text{ cal/g} \cdot \text{mole}$$
$$R = 1.987 \text{ cal/g} \cdot \text{mole} \cdot {}^\circ\text{k}, \; T = 294^\circ\text{K} \tag{50}$$

Inserting the value of D_m^c into the first of equations (46) yields D and together with the first of equations (44) gives $\mathcal{D}$, i.e.,

$$D = 7.72242 \times 10^{-7} \text{ cm}^2/\text{hr}, \; \mathcal{D} = 1.05541 \times 10^{-5} \text{ cm}^2/\text{hr} \tag{51}$$

There remains the determination of λ and ν. Combining the second of equations (44) with (45), the constant Q_o can be solved:

$$Q_o = \sqrt{\frac{\rho c_p \lambda \nu R T_o^2}{u C_o}} = 9.55650 \times 10^5 \text{ m}^2/\text{s}^2 \tag{52}$$

in which $C_o = 18.484$ Kg and $\rho = 1{,}590$ Kg for the T300/5208 composite [14]. The second of equations (44) and (45) now yield

$$\lambda = 0.03235 \text{ kg} \cdot \text{m}^{-3}/{}^\circ\text{C}, \; \nu = 0.75389^\circ\text{C/kg} \cdot \text{m}^{-3} \tag{53}$$

This completes the numerical evaluation of D, $\mathcal{D}$, λ and ν for the case of plane stress.

It follows immediately from equations (24) that

$$D_m = 7.91547 \times 10^{-7} \text{ cm}^2/\text{hr}, \quad D_h = 1.08179 \times 10^{-5} \text{ cm}^2/\text{hr} \tag{54}$$

When deformation is coupled with diffusion, the additional constant N given by the third of equations (27) must be evaluated. Knowing that $\alpha = 31.3 \times 10^{-6}$ and $\nu_p = 0.33$ as given in Table 1, and E = 67.155 GPa and c_p as computed by equations (38) and (41), the value

$$N = 7.60997 \times 10^{-9} \text{ ms}^2\text{°C/Kg} \tag{55}$$

is evaluated for plane stress. A glance at the six expressions in equations (25) to (27) show that the remaining six unknowns d_c, d_t, A, L_{11}, L_{12} and L_{22} can be obtained without difficulty. Their values are

$$\begin{aligned} d_c &= 1{,}230.33 \text{ m}^5/\text{Kgs}^2 \\ d_t &= -3{,}330.931 \text{ m}^2/\text{s}^2\text{°C} \\ A &= -2{,}257.93 \text{ m}^2/\text{s}^2\text{°C} \end{aligned} \tag{56}$$

and the Onsager coefficients are given by

$$\begin{aligned} L_{11} &= 3.13576 \times 10^{-18} \text{ Kg·s/m}^3 \\ L_{12} &= 4.93980 \times 10^{-12} \text{ Kg/m·s} \\ L_{22} &= 7.19903 \times 10^{-4} \text{ Kg·m/s}^3 \end{aligned} \tag{57}$$

The above numerical evaluation is based on the best approximation by assuming that

L_{22} remains unchanged as D_m, D_h, λ and ν are matched* with those obtained from the classical theory where moisture and temperature are uncoupled. Alternatively, L_{12} may be assumed to remain unchanged which will lead to a slightly different value of A.

Coupled Constants for Plane Strain. The conversion to plane strain can be made in a straightforward manner. First, the constants α^*, β^*, ν_p^* and E^* can be computed from equations (30):

$$\alpha^* = 4.15353 \times 10^{-5}/°C, \quad \beta^* = 3.5912 \times 10^{-3}/\text{wt\% } H_2O$$

$$\nu_p^* = 0.493, \quad E^* = 75.9328 \times 10^9 \text{ N/m}^2 \tag{58}$$

With the aid of equations (31), the remaining quantities are also obtained:

$$c_p^* = 785.1243 \text{ m}^2/\text{s}^2°C$$

$$d_c^* = 7{,}013.8 \text{ m}^5/\text{Kgs}^2 \tag{59}$$

$$d_t^* = -3{,}330.6 \text{ m}^2/\text{s}^2°C$$

Following the definition given by the third of equations (27), N^* is obtained

$$N^* = \alpha^* \left[\frac{\rho c_p^*}{T_o} - \frac{2E^*\alpha^{*2}}{1-\nu_p^*}\right]^{-1} = 1.12402 \times 10^{-8} \text{ ms}^2°C/\text{Kg} \tag{60}$$

*The coupling constants are determined by matching the theoretical boundary value solution for a problem with very weak coupling to the experimental data without the influence of coupling. Since the physical constants, once determined, are independent of boundary conditions, they can be used in general for problems where coupling influence is significant.

Similarly, equations (25) in terms of plane strain render

$$D_m^* = \left(\frac{2E^*\beta^*}{1-\nu_p^*} + d_c^*\right)L_{11} = 2.59555 \times 10^{-6} \text{ cm}^2/\text{hr}$$

$$D_h^* = (A^*T_oL_{11} + \frac{1}{T_o} L_{22} + 2L_{12})(A^*/T_o)/\left(\frac{\rho c_p^*}{T_o} - \frac{2E^*\alpha^{*2}}{1-\nu_p^*}\right) \tag{61}$$

$$= 1.26108 \times 10^{-5} \text{ cm}^2/\text{hr}$$

in which A^* is obtainable from equation (26) as

$$A^* = \frac{2E^*\alpha^*\beta^*}{1-\nu_p^*} + d_t^* = -\ 392.183 \text{ m}^2/\text{s}^2\cdot^\circ\text{C} \tag{62}$$

Therefore, λ^* and ν^* follow from equations (27):

$$\lambda^* = (L_{11}A^* + \frac{1}{T_o} L_{12})/D_h^* = 0.04454 \text{ Kg} \cdot \text{m}^{-3}/^\circ\text{C}$$

$$\nu^* = \left(\frac{1}{T_o}\frac{L_{21}}{L_{11}} + A^*\right)/\left(\frac{\rho c_p^*}{T_o} - \frac{2E^*\alpha^{*2}}{1-\nu_p^*}\right) = 1.34389 \ ^\circ\text{C/Kg} \cdot \text{m}^{-3} \tag{63}$$

Finally, D^* and $\mathcal{D}^*$ can be calculated as

$$D^* = (1-\lambda^*\nu^*)D_m^* = 2.44018 \times 10^{-6} \text{ cm}^2/\text{hr}$$

$$\mathcal{D}^* = (1-\lambda^*\nu^*)D_h^* = 1.18559 \times 10^{-5} \text{ cm}^2/\text{hr} \tag{64}$$

The constants in equations (63) and (64) will be used subsequently for analyzing the transient hygrothermal stresses around a circular hole in a stretched plate.

TRANSIENT DIFFUSION AND STRESS DISTRIBUTION NEAR CIRCULAR HOLE

Consider the problem of a circular hole of radius, a, in a square plate with dimensions LxL as shown in Figure 1. The boundary conditions on the hole Γ_I consist of sudden rise in moisture or temperature and are independent of the polar angle θ. A uniform stress of magnitude σ_0 is applied in the y-direction on Γ_{II} such that only the shaded area need to be analyzed. It is of interest to investigate the interaction between the stresses induced by diffusion and those by mechanical loading.

Finite Element Analysis. The basic time-dependent finite element formulation follows that in [15] for the case when the deformation is uncoupled from the diffusion process. The governing differential equations correspond to those in equations (32) which are similar to equations (22) except for R being replaced by T as $\phi = 0$. Without going into details, it should be mentioned that the variational calculus formulation in [15] is unique because the time dependent portion of the problem is solved analytically as an eigenvalue problem by application of Laplace transform in the time variable. This choice is also adopted in this work and will not be elaborated further. Referring to Figure 2 for the finite element grid pattern layout in the first quadrant. A total of 139 triangular elements and 87 nodes are used. Computations are carried out by letting a = 1.0 and L = 4.0.

For the convenience of numerical computation, the first two expressions of equations (22) are cast into dimensionless forms:

$$\frac{D^*}{\varepsilon} \nabla^2 C = \frac{\partial}{\partial \tau} (C - \lambda^* R)$$

$$\frac{D^*}{\varepsilon} \nabla^2 R = \frac{\partial}{\partial \tau} (R - \nu^* C) \qquad (65)$$

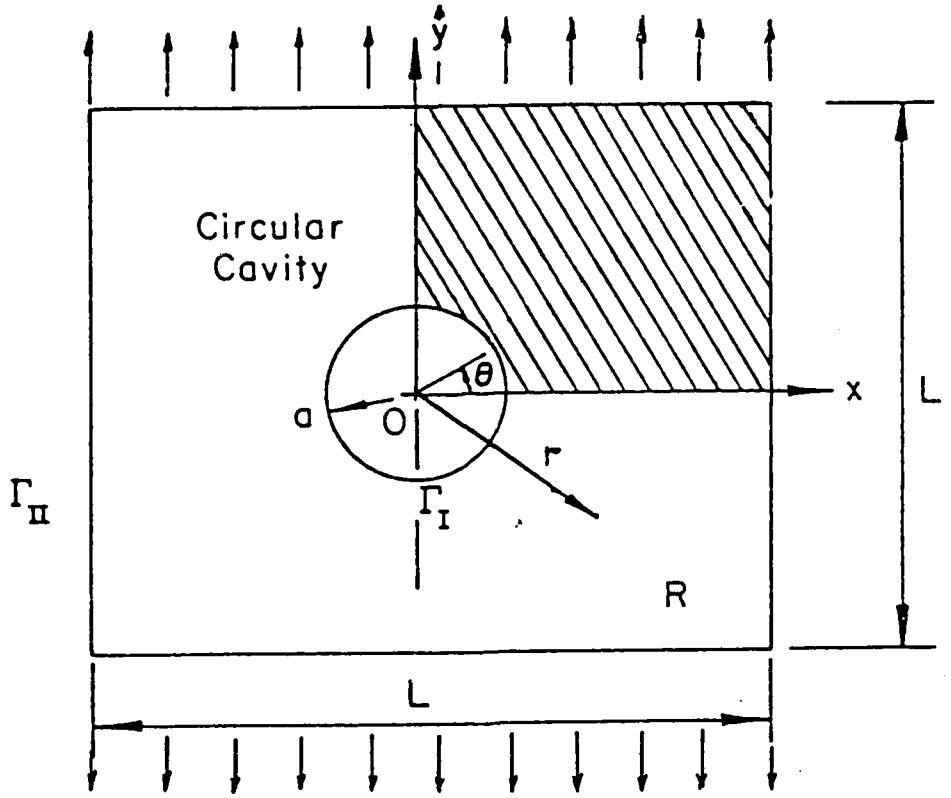

Figure 1 - Circular hole in a stretched plate

in which $\tau = \varepsilon t/h^2$ is the normalized time parameter with ε being a time scale factor and h the plate thickness. The space variables in the Laplacian operator ∇^2 are normalized with reference to h, i.e., x/h, y/h and z/h. The time scale factor ε is chosen, respectively, as 10^{-5} cm^2/hr and 1.0 cm^2/hr for suddenly applied moisture and temperature boundary conditions.

Sudden Moisture Rise. Let the initial conditions of moisture and temperature on Γ_I and Γ_{II} be such that

$$\Delta C = \begin{cases} \Delta C_B, \text{ on } \Gamma_I \\ 0 \quad , \text{ on } \Gamma_{II} \end{cases} \qquad (66)$$

$$\Delta T = 0, \text{ on } \Gamma_I \text{ and } \Gamma_{II}$$

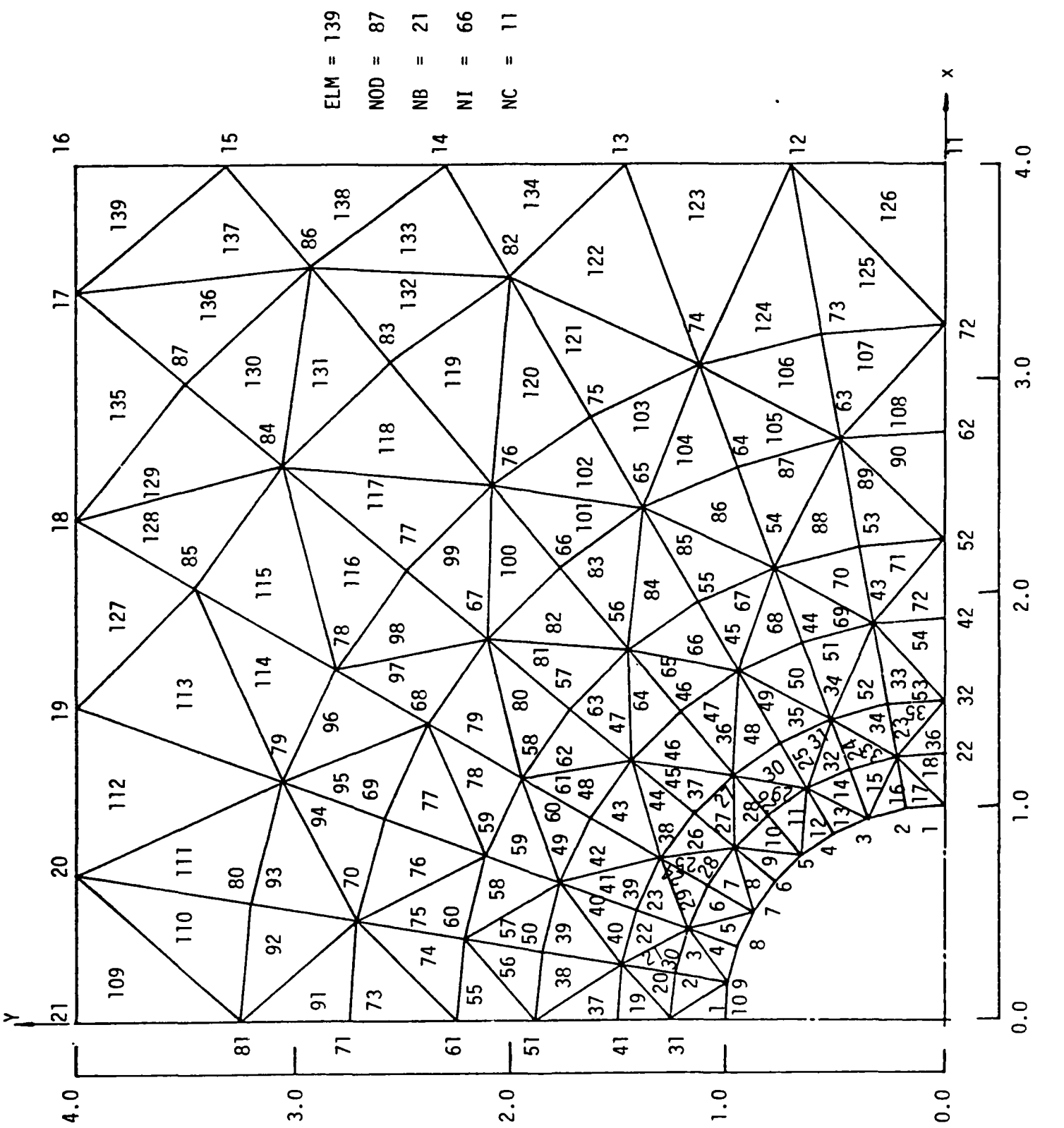

Figure 2 - Grid pattern for rectangular plate with a circular cavity

More specifically, the moisture and temperature on Γ_{II} are kept constant at 0% RH and 21°C, respectively, at all time t while the moisture on Γ_I is raised from 0% to 75% RH at constant temperature. Results for a constant applied stress of $\sigma_0 = 5 \times 10^7$ N/m^2 are first presented while the influence of raising σ_0 to 10^8 N/m^2 will be discussed only in terms of the strain energy density function.

Let the average moisture and temperature be weighed through the volume of each triangular element as follows:

$$\overline{C} = \frac{1}{V} \int C dv, \quad \overline{T} = \frac{1}{V} \int T dv \tag{67}$$

In the sequel, all solid curves refer to stress coupling while the dotted curves correspond to stress uncoupling. Moisture and temperature are always coupled. Figure 3 gives a plot of $(\overline{C}-C_0)$% dry weight against τ. The coupled solution can

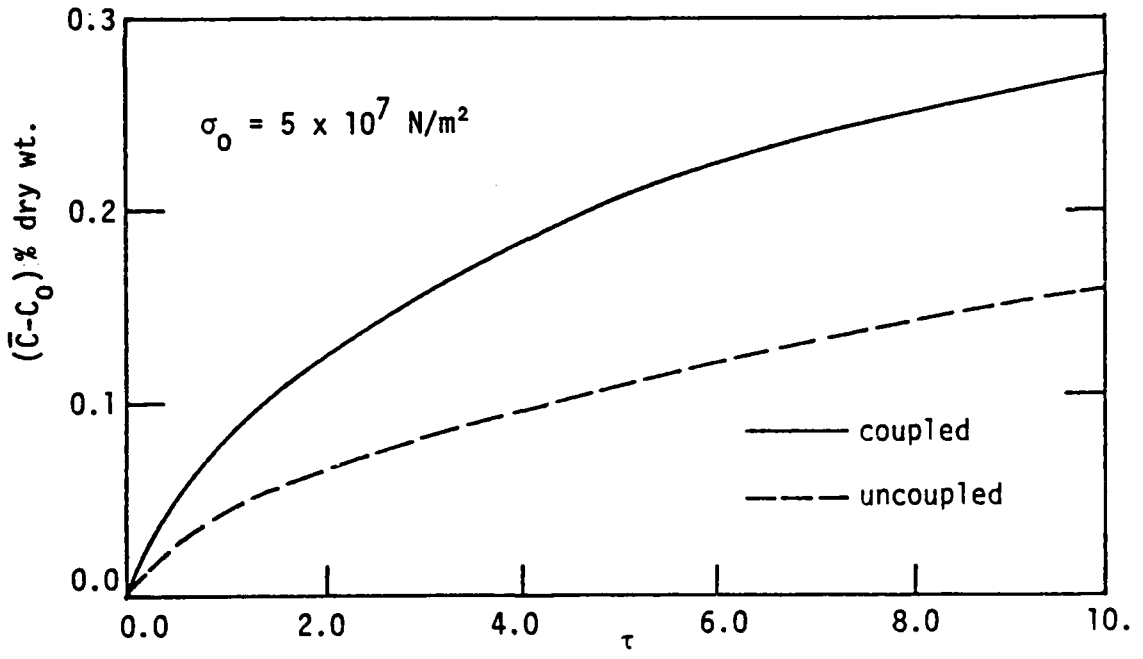

Figure 3 - Average moisture gain for sudden moisture change on circular cavity from 21°C 0% to 75% RH. Material T300/5208 graphite/epoxy laminates

be 40% to 50% higher than the uncoupled solution. The average temperature change $(\overline{T}-T_o)$ as a function of τ is displayed in Figure 4. Note that $(\overline{T}-T_o)$ decreases at first and then rises sharply* while the corresponding results without stress coupling remains virtually constant with respect to time. Figures 5 and 6 ex-

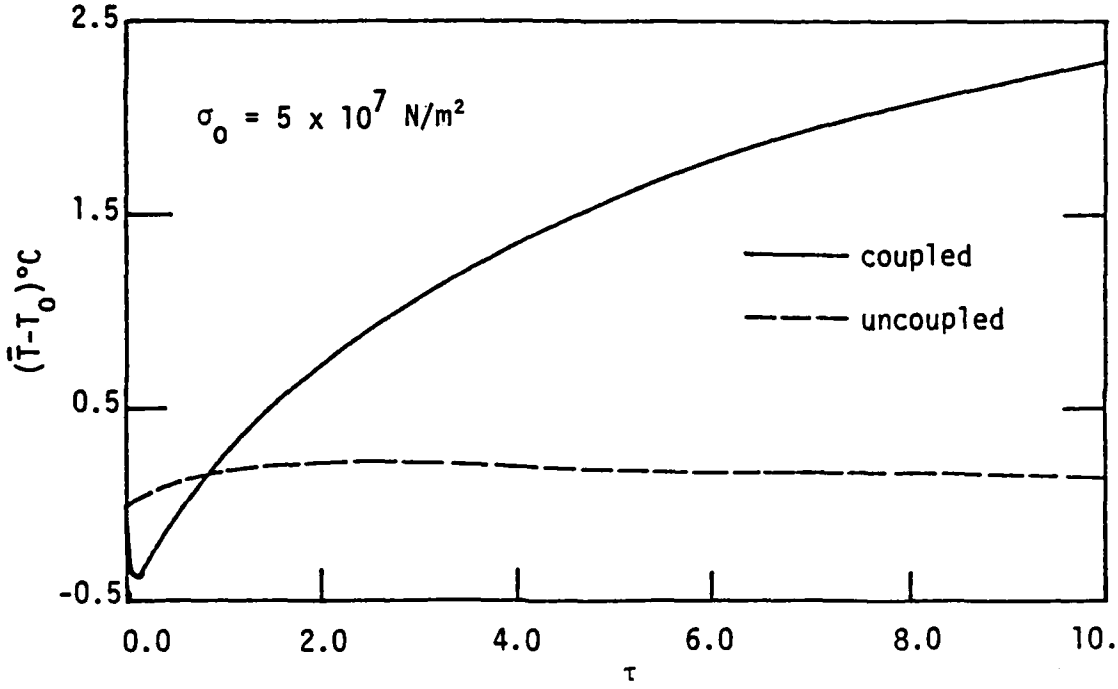

Figure 4 - Average temperature rise for sudden moisture change on circular cavity from 21°C 0% to 75% RH. Material T300/5208 graphite/epoxy laminates

hibit the change of $(\overline{C}-C_o)$ % dry weight and $(\overline{T}-T_o)$ with the normalized radial distance r/a for τ = 1.0. It is seen from Figure 5 that the average moisture content decreases with increasing distance r/a. The stress coupling effect only changed the results quantitatively and not qualitatively in that the solid curves are always higher than the dotted curves for a given r/a value but the remained constant for all θ. The uniaxial stress level of σ_o = 5 x 10^7 N/m² is not strong enough to influence the asixymmetric character of $\overline{C}-C_o$ which is dominated by the initial moisture and temperature boundary conditions. On the other hand, the average temperature change $(\overline{T}-T_o)$ in Figure 6 is seen to be strongly affected by stress

*This transient effect becomes more pronounced when the temperature difference $(\overline{T}-T_o)$ at the nodal points are plotted as a function of time [16].

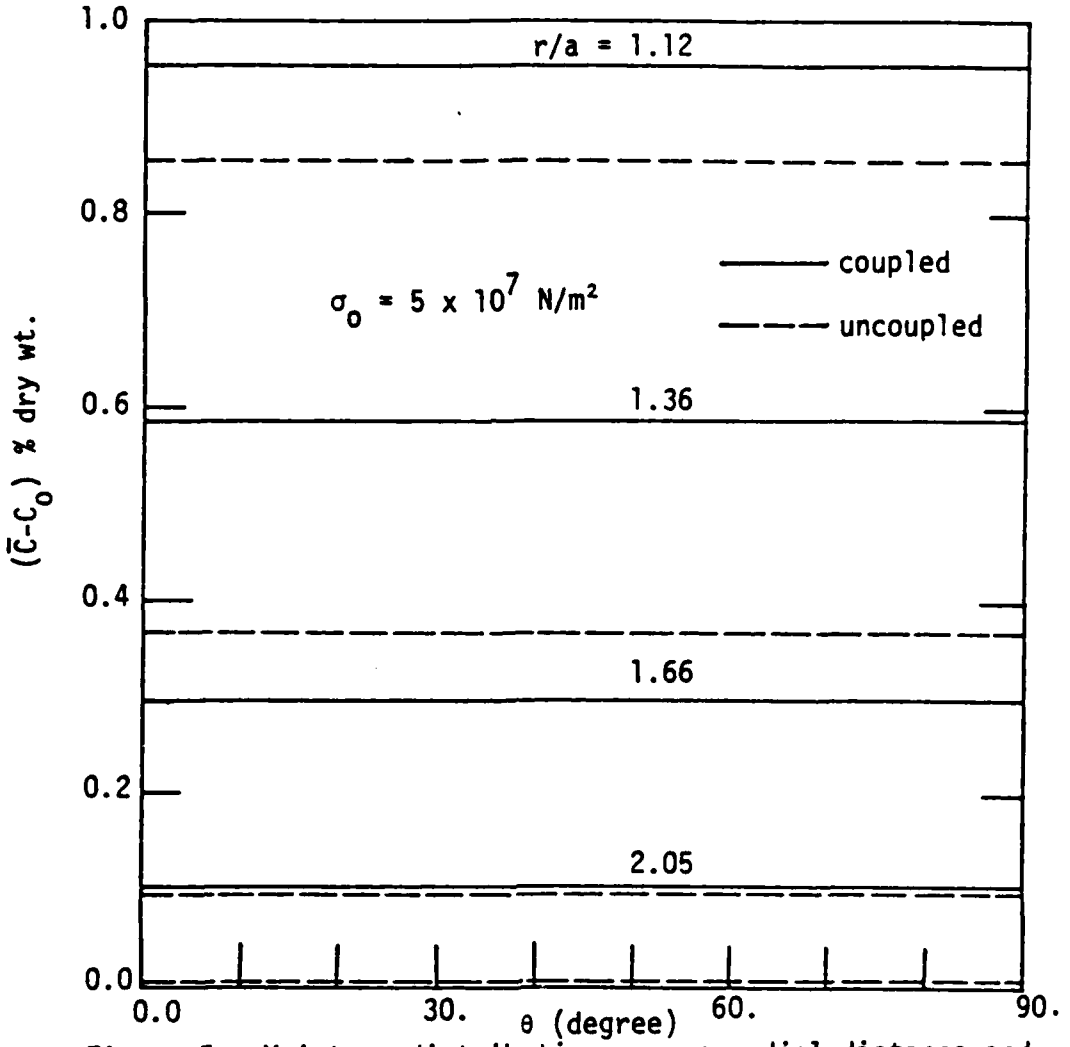

Figure 5 - Moisture distribution versus radial distance and angle at $\tau = 1.0$ for sudden moisture change on circular cavity

coupling both quantitatively and qualitatively. Axisymmetry of the initially prescribed temperature conditions is clearly disturbed with $(\bar{T}-T_o)$ exhibiting minima between $\theta = 50°$ and 60° as r/a is varied from 1.36 to 1.66. The variations of moisture and temperature with distance* r/a along the x-axis are shown in Figures 7 and 8. While the moisture change in Figure 7 decreases monotonically with r/a with increasing deviation between the coupled and uncoupled solution as τ increased, the temperature change in Figure 8 tends to oscillate reaching a maximum near the hole and then decay rapidly to the prescribed value on the boundary Γ_{II}.

*The distance r and angle θ are average over two adjacent triangular elements enclosed by the radial and circular lines in Figure 2.

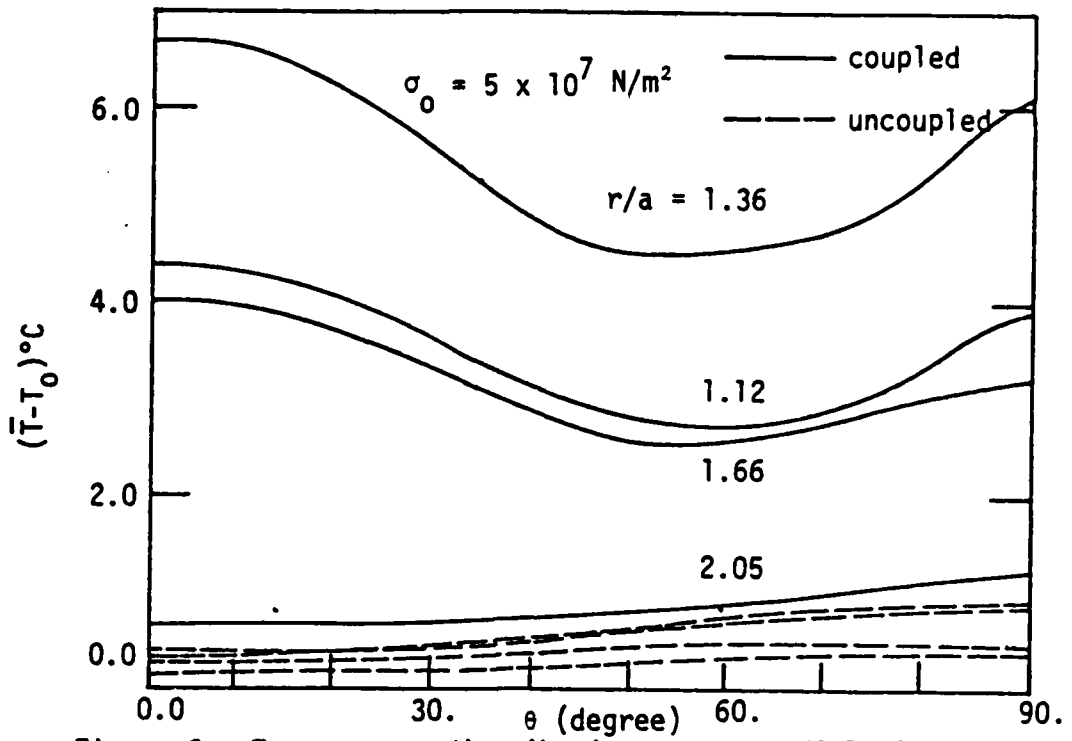

Figure 6 - Temperature distribution versus radial distance and angle at $\tau = 1.0$ for sudden moisture change on circular cavity

The time-dependent stress components σ_x, σ_y, σ_z and σ_{xz} are plotted as a function of r/a for different time τ in Figures 9 to 12 inclusive. All the normal stresses σ_x, σ_y and σ_z can be tensile or compressive depending on the time elapsed and they do exhibit a significant difference from the uncoupled theory. The stress component σ_x in Figure 9 is seen to be predominantly compressive for $\tau > 0.24$. It became tensile for $\tau \simeq 0.04$ at $r/a \simeq 1.75$ and diminished to zero on Γ_{II}. The maximum value of σ_x at $\tau = 7.5$ is -42.5 N/m² for the coupled case and -37.5 N/m² for the uncoupled case. Referring to Figure 10, σ_y is mostly tensile except for those locations near the hole boundary. The applied mechanical stress $\sigma_o = 5 \times 10^7$ N/m² is seen to have little influence on σ_y which rises to a maximum near the hole rather than decaying monotonically with $(\sigma_y)_{max}$ at r/a = 1.0 if σ_o were the only external loading.

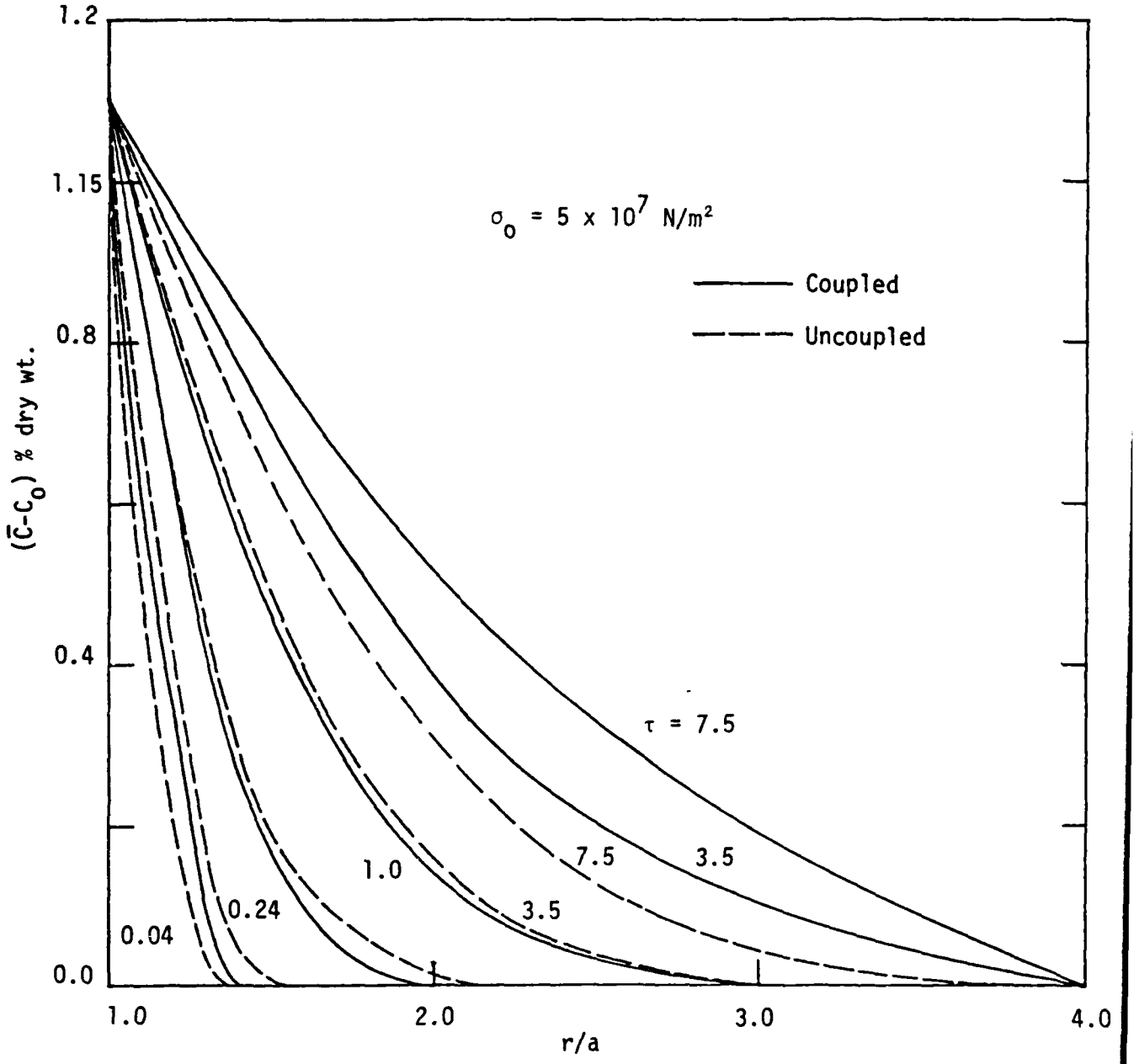

Figure 7 - Variation of moisture versus distance along x axis for sudden moisture change on circular cavity. Material T300/5208 laminates

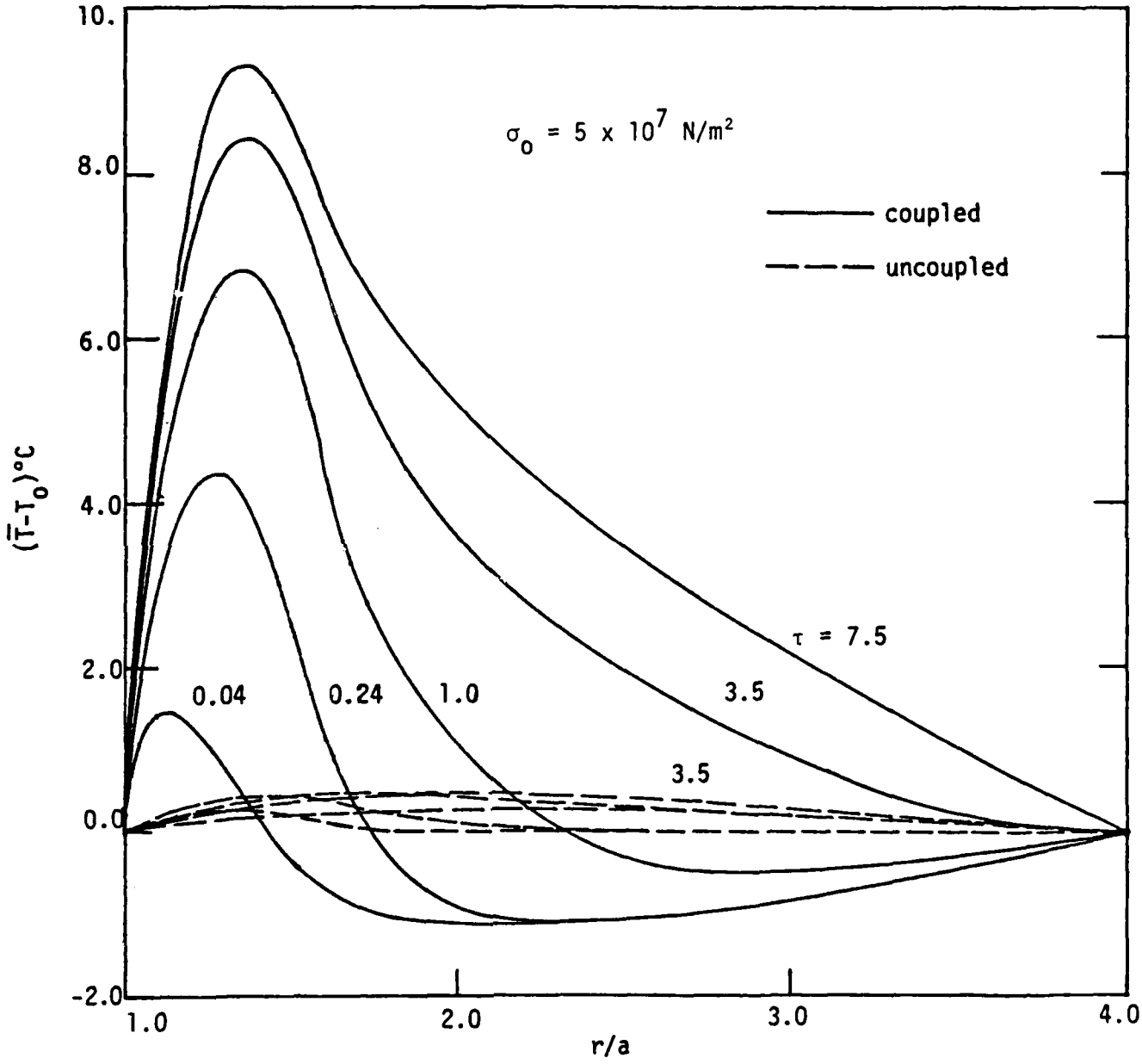

Figure 8 - Variation of temperature versus distance along x axis for sudden moisture change on circular cavity. Material T300/5208 laminates

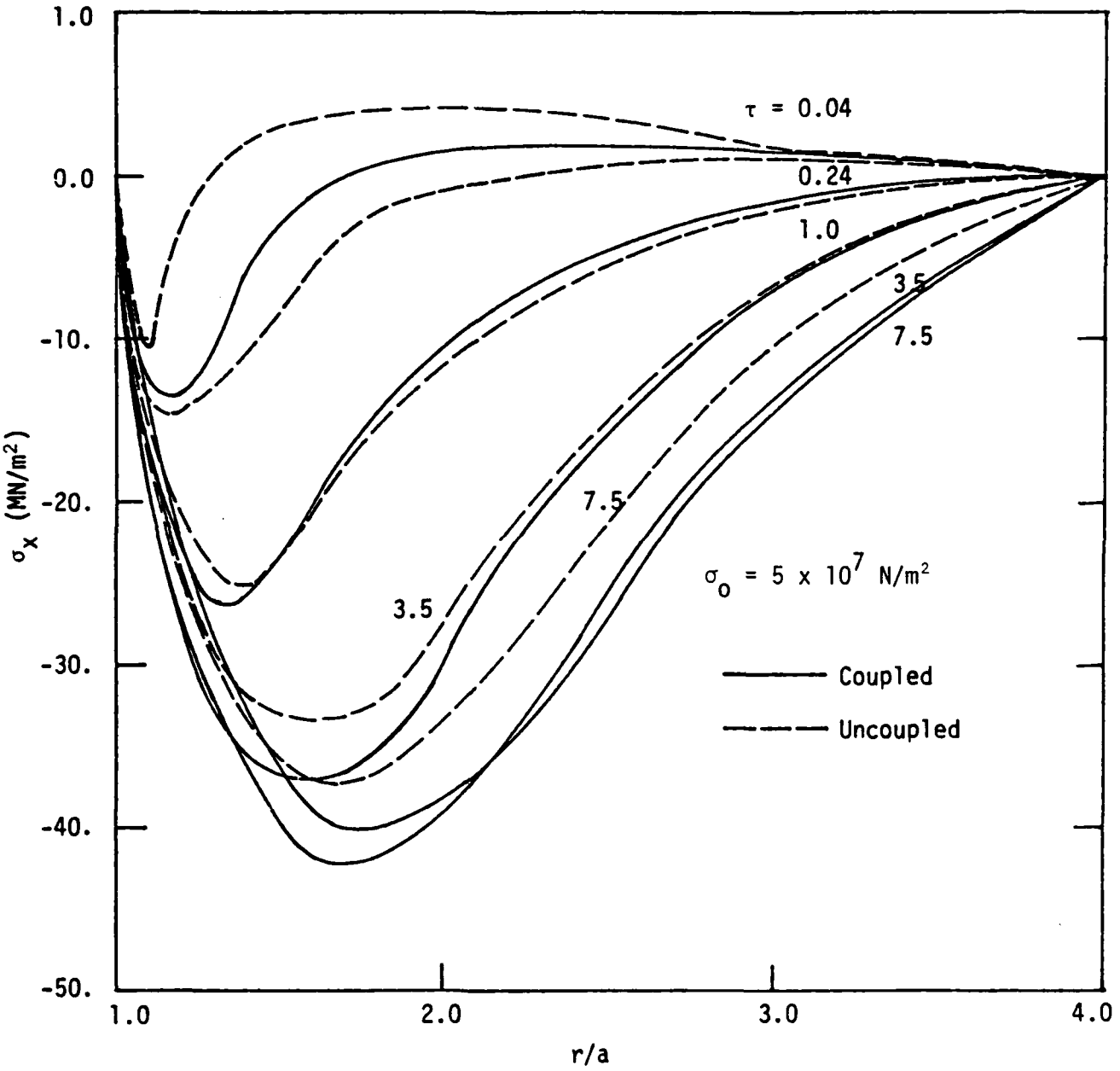

Figure 9 - Variation of stress σ_x versus distance along x axis for sudden moisture change on circular cavity. Material T300/5208 laminates

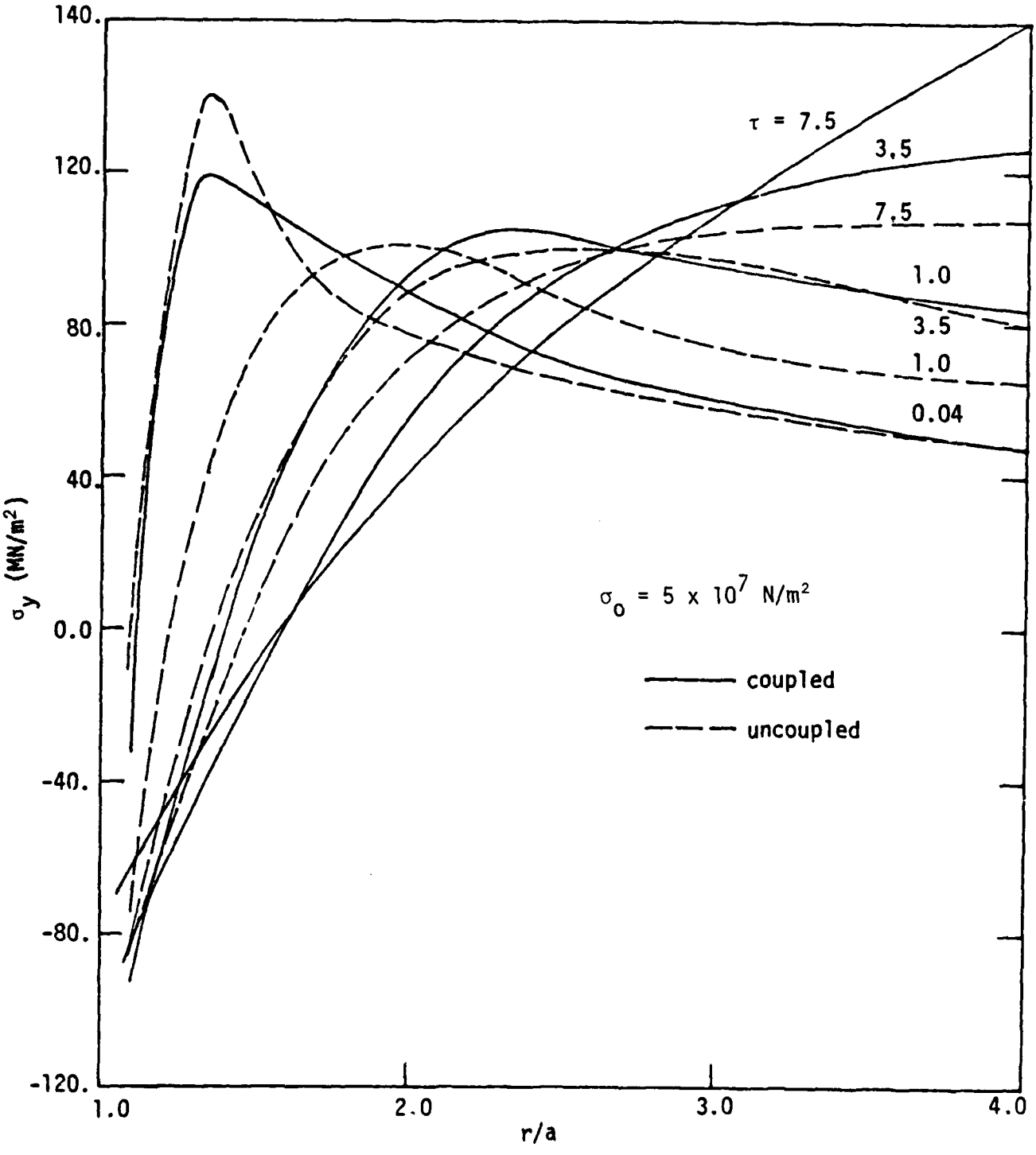

Figure 10 - Variation of stress σ_y versus distance along x axis for sudden moisture change on circular cavity. Material T300/5208 laminates

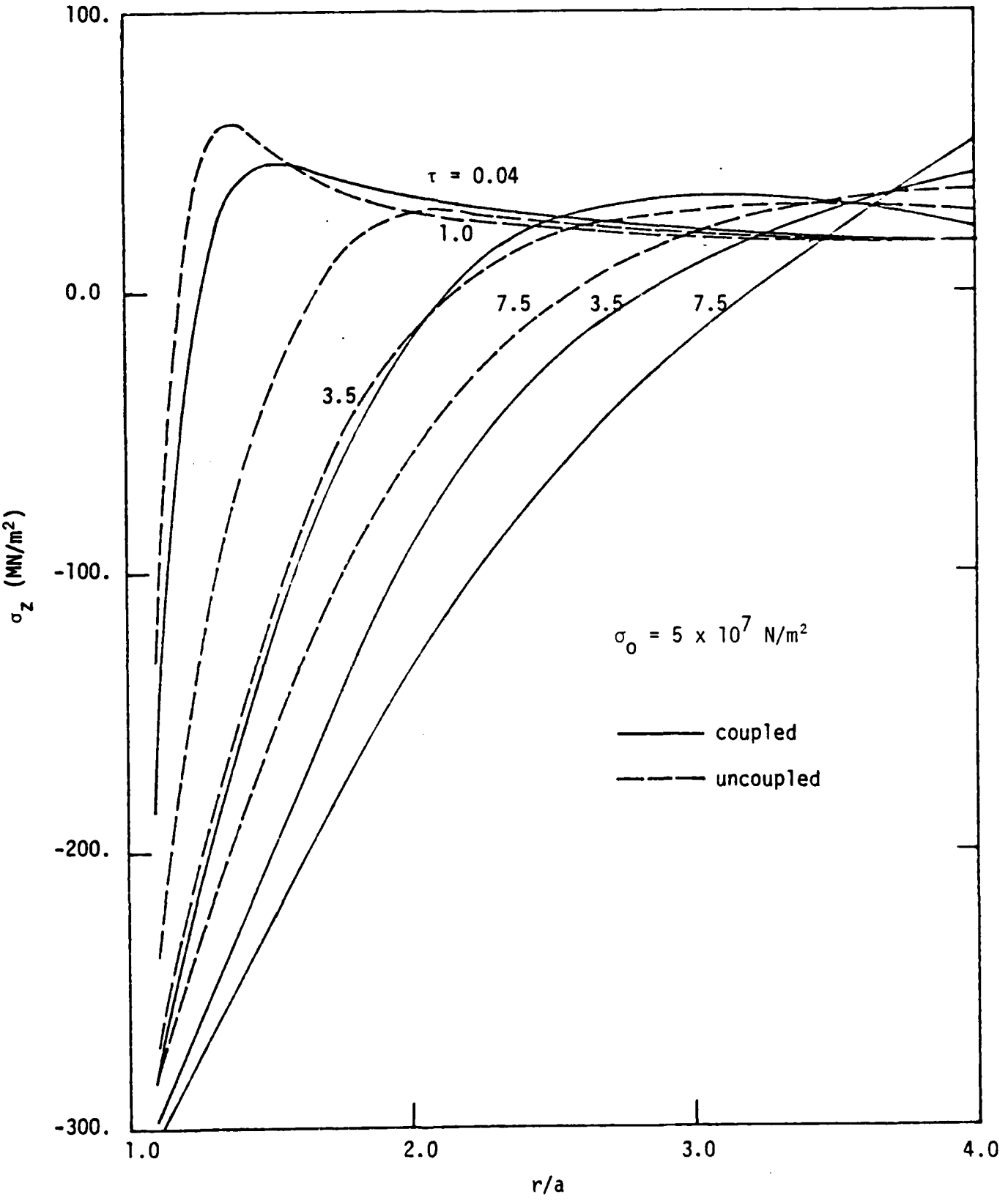

Figure 11 - Variation of stress σ_z versus distance along x axis for sudden moisture change on circular cavity. Material T300/5208 laminates

The behavior of σ_z is given in Figure 11 which is highly compressive for small values of r/a and becomes tensile as r/a is increased. The shear stress component σ_{xy} in Figure 12 remained constant for most of the part of the x-axis. Only small fluctuations are observed near the hole. In general, deformation coupling tends to increase the magnitude of the local stresses depending, of course, on the time τ.

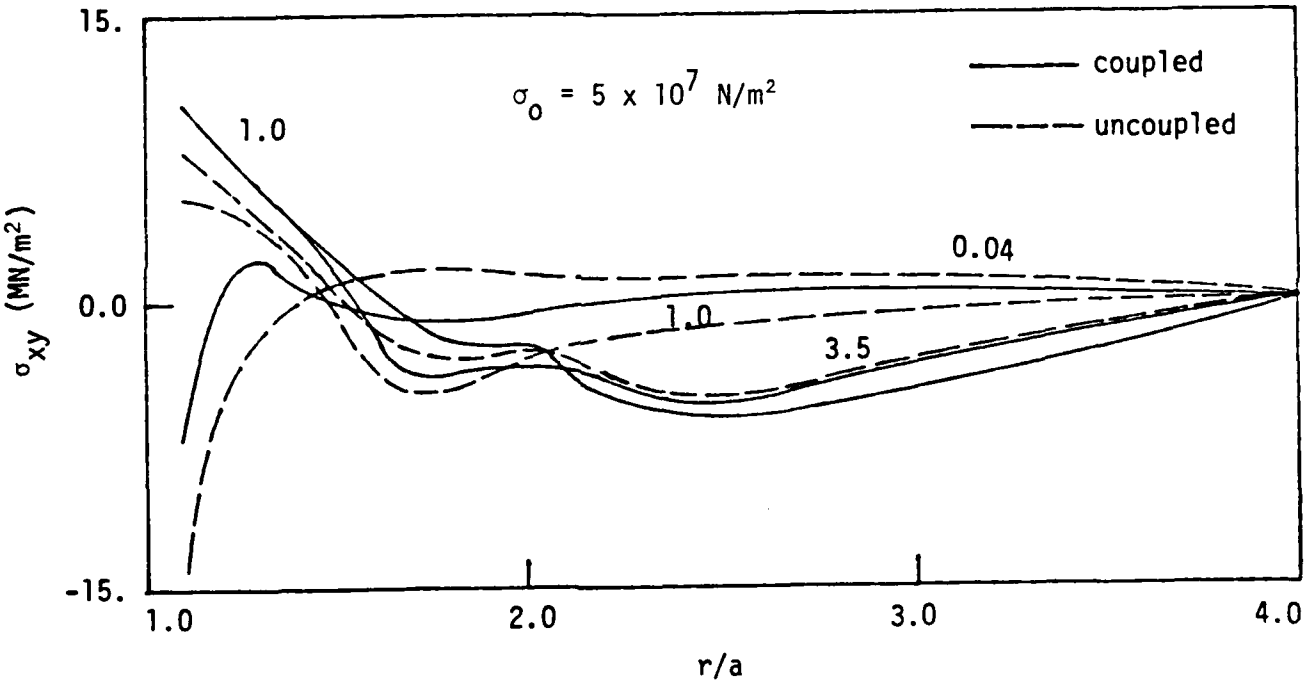

Figure 12 - Variation of shearing stress versus distance along x axis for sudden moisture change on circular cavity. Material T300/5208 laminates

Sudden Temperature Rise. Suppose that the temperature on the hole Γ_I is now increased suddenly while the moisture is kept constant. The following conditions then prevail:

$$\Delta C = 0, \text{ on } \Gamma_I \text{ and } \Gamma_{II}$$

$$\Delta T = \begin{cases} \Delta T_B, \text{ on } \Gamma_I \\ 0 \quad , \text{ on } \Gamma_{II} \end{cases} \tag{68}$$

Again, the moisture, temperature and stress conditions on Γ_{II} are maintained unchanged as initially specified at 21°C and 75% RH. The applied stress σ_o in the y-direction is 10^8 N/m^2.

As the temperature on Γ_I is raised from 21°C to 61°C with the moisture kept constant at 75% RH. hygrothermal stresses will be induced and fluctuate with time. The same T300/5208 composite material properties as those given earlier will be used to calculate the numerical results.

Figure 13 gives a plot of the average moisture change $(\overline{C}-C_o)$ expressed in terms of % of dry weight of the laminate against the dimensionless time parameter τ. The time scale factor ε in τ is chosen as 1.0 cm^2/hr for the present problem of sudden temperature change as specified by the conditions in equations (68). The solid curve indicates that more moisture is first gained by the composite when stress coupling effect is taken into account. The moisture content then decreases as time increases. The peak of the solid curve is higher than that of the dotted

curve and it occurs at a smaller value of τ. The average temperature $(\bar{T}-T_o)$ in

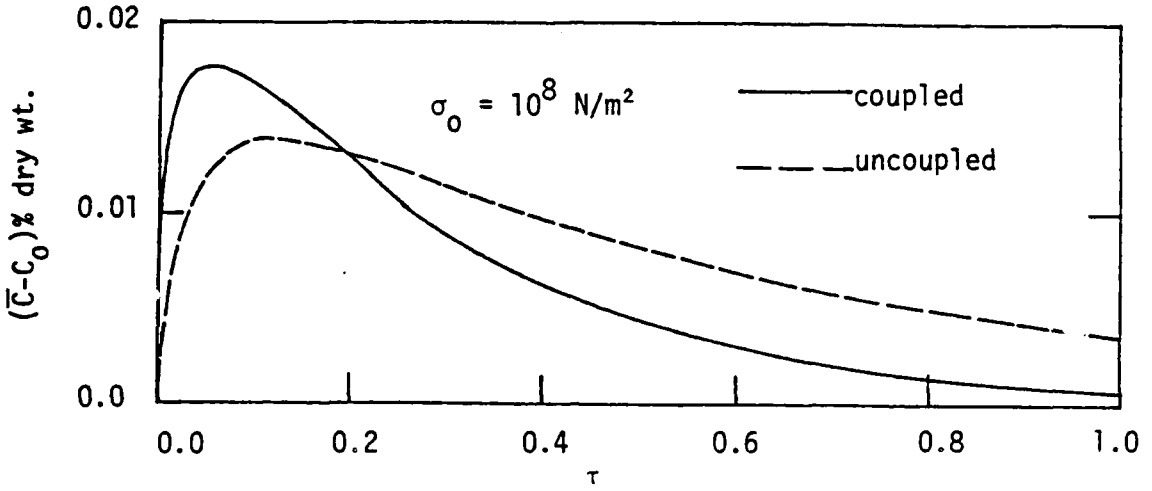

Figure 13 - Average moisture gain versus time for sudden temperature change on circular cavity from 21°C to 61°C at 75% RH. Material T300/5208 graphite/epoxy laminate

Figure 14 is seen to rise quickly to a steady state. This occurs at $\tau = 0.25$ and 0.50 for the cases without and with stress coupling, respectively. Similar

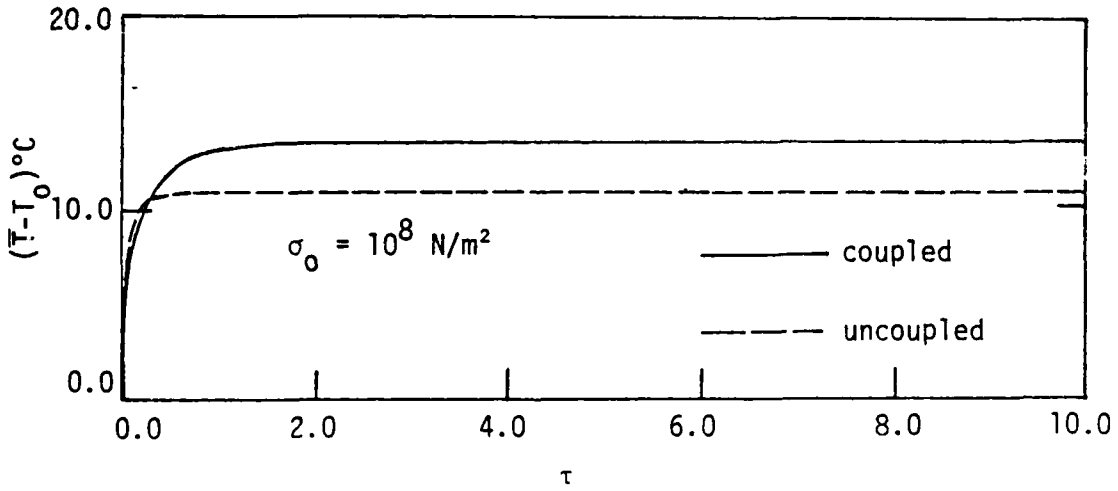

Figure 14 - Average temperature rise versus time for sudden temperature change on circular cavity from 21°C to 61°C at 75% RH. Material T300/5208 graphite/epoxy laminate

plots are displayed in Figures 15 and 16 to show the variations of $(\bar{C}-C_o)$ and $(\bar{T}-T_o)$ with the polar angle ϑ. Deviations from axisymmetry become more pro-

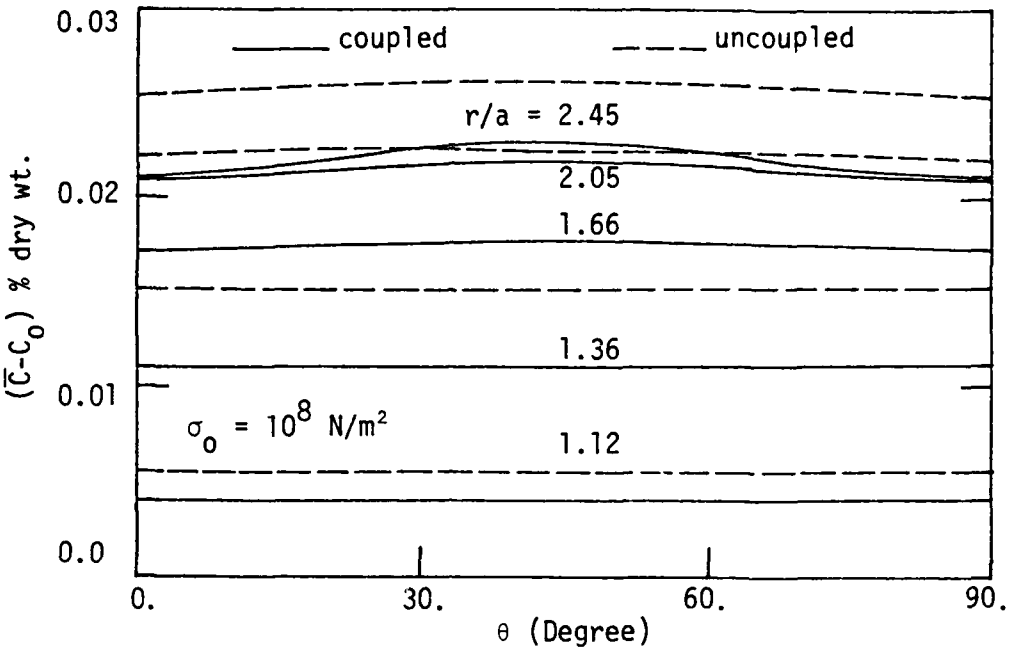

Figure 15 - Moisture distribution at $\tau = 0.2$ versus angle θ from x-axis for different r/a. Sudden temperature change on circular cavity from 20°C to 61°C at 75% RH

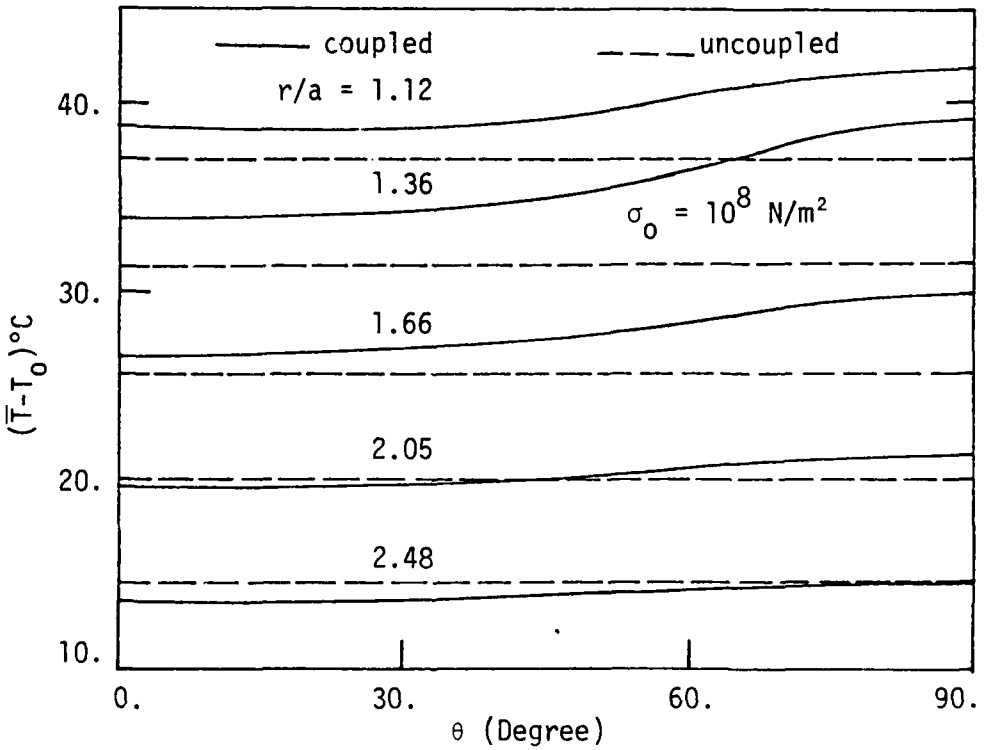

Figure 16 - Temperature distribution at $\tau = 0.2$ versus angle θ from x-axis for different r/a. Sudden temperature change on circular cavity from 21°C to 61°C at 75% RH

nounced for $(\overline{C}-C_o)$ as r/a is increased while the opposite trend is observed for $(\overline{T}-T_o)$. It is of interest to note that $(\overline{C}-C_o)$ increases rapidly to a peak for small τ near the hole, i.e., $r \simeq a$ and then it decreases sharply to zero, Figure 17. This effect dies out with time as it is to be expected. The average temperature change $(\overline{T}-T_o)$ varied monotonically with r/a for small time and then it acquires a small peak for $\tau > 0.1$ before it decays rapidly. This is shown in Figure 18.

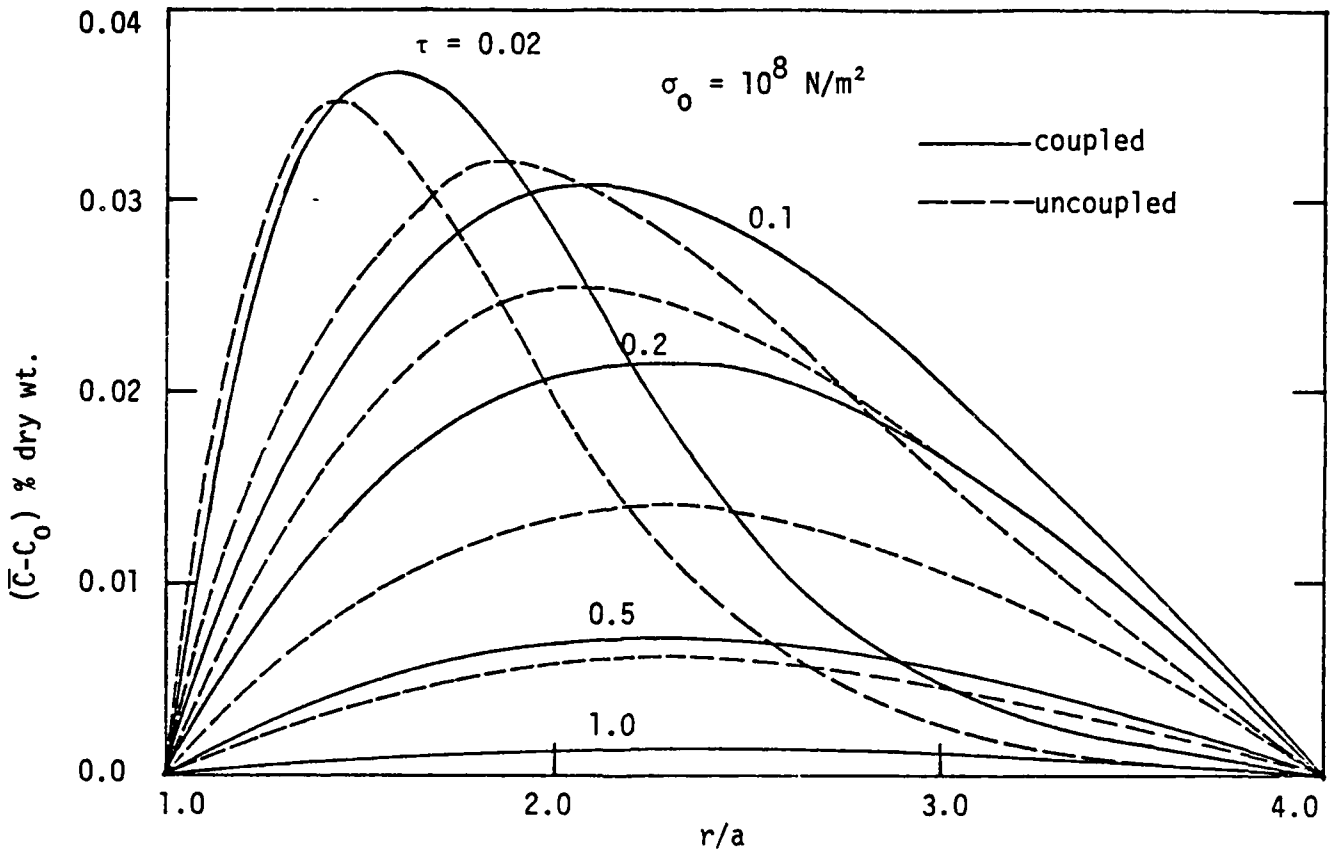

Figure 17 - Variation of moisture versus distance along x axis for sudden temperature change on circular cavity. Material T300/5208 laminate

The results in Figures 19 to 22 inclusive pertain to plots of σ_x, σ_y, σ_z and σ_{xy} against r/a for different time τ. The stress component σ_x acquires a peak near the hole before it decreases in magnitude as indicated in Figure 19.

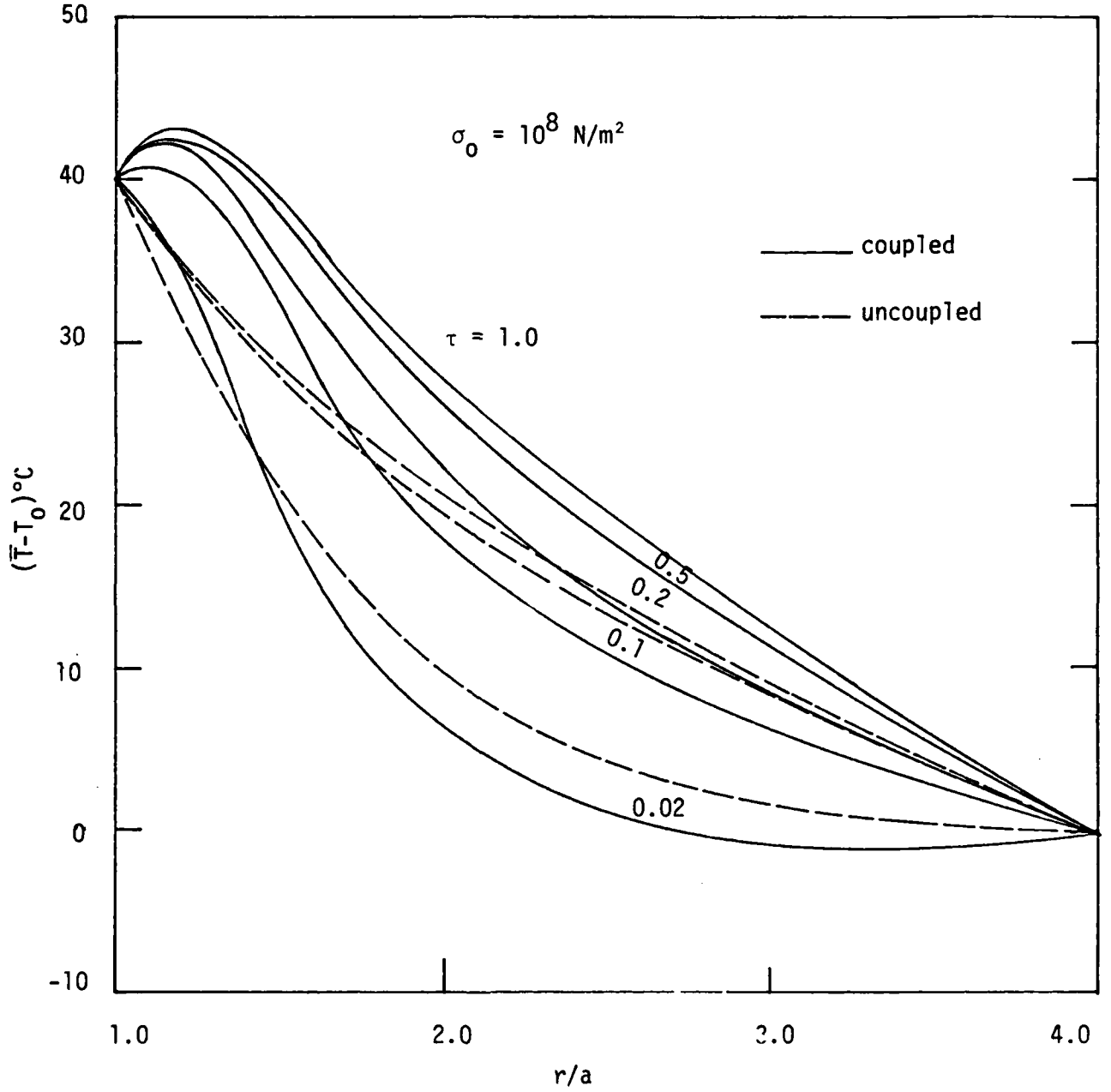

Figure 18 - Variation of temperature versus distance along x axis for sudden temperature change on circular cavity. Material T300/5208 laminate

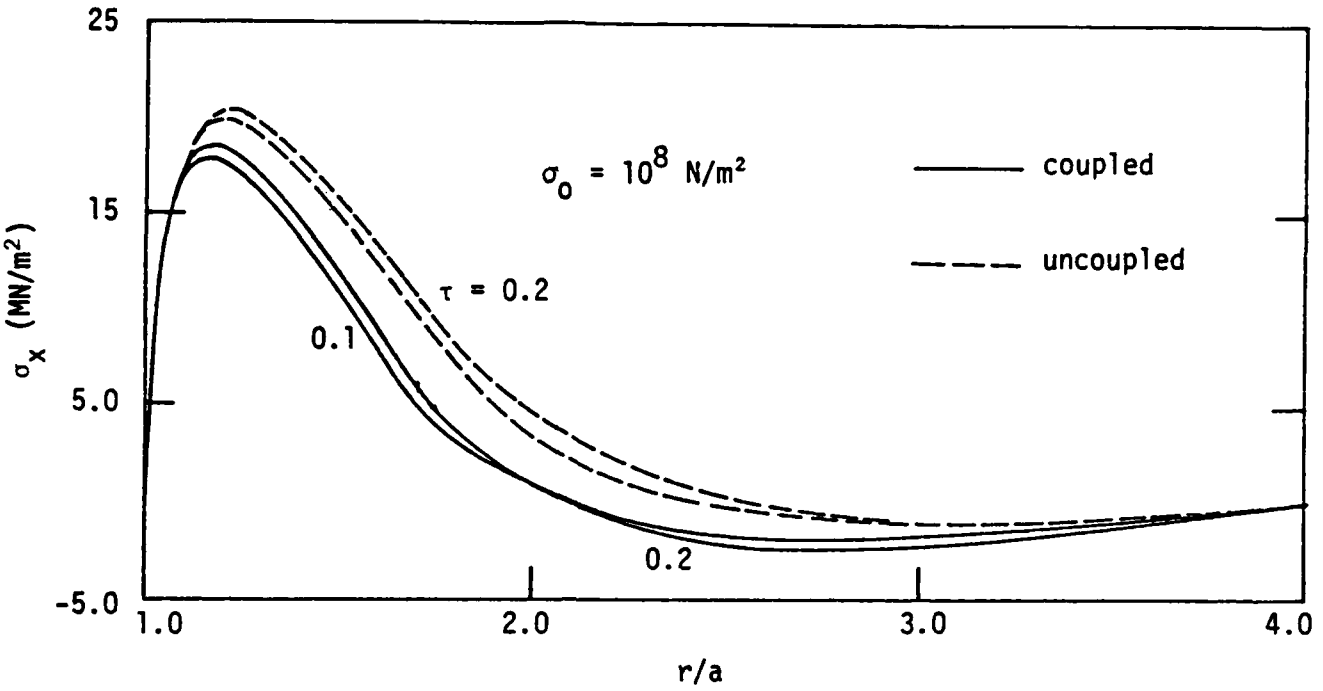

Figure 19 - Variation of stress σ_x versus distance along x axis for sudden temperature change on circular cavity. Material T300/5208 laminate

For an applied stress level of $\sigma_o = 10^8$ N/m^2, stress coupling tends to lower the peak value of σ_x. Figure 20 shows that σ_y decreases with r/a and the solid curves become larger in magnitude than the dotted curves at r/a $\simeq$ 1.75. The dominance of mechanical loading is clearly exhibited when σ_o is increased from 5 x 10^7 N/m^2 in Figure 10 to 10^8 N/m^2 in Figure 20. Note that the maximum of σ_y now occurs at r/a = 1.0 and decays as r/a is increased. The stress component σ_z displayed graphically in Figure 21 reveals that it is compressive near the hole and then becomes tensile at r/a > 2.3. Stress coupling does not seem to influence the shear stress σ_{xy} as the dotted and solid curves in Figure 22 almost coincide with each other.

FAILURE SITE PREDICTION: STRAIN ENERGY DENSITY CRITERION

The strain energy density criterion [6,7] has been used in many applications for predicting the sites of failure initiation. This is accomplished by computing for the stationary values of dW/dV given by

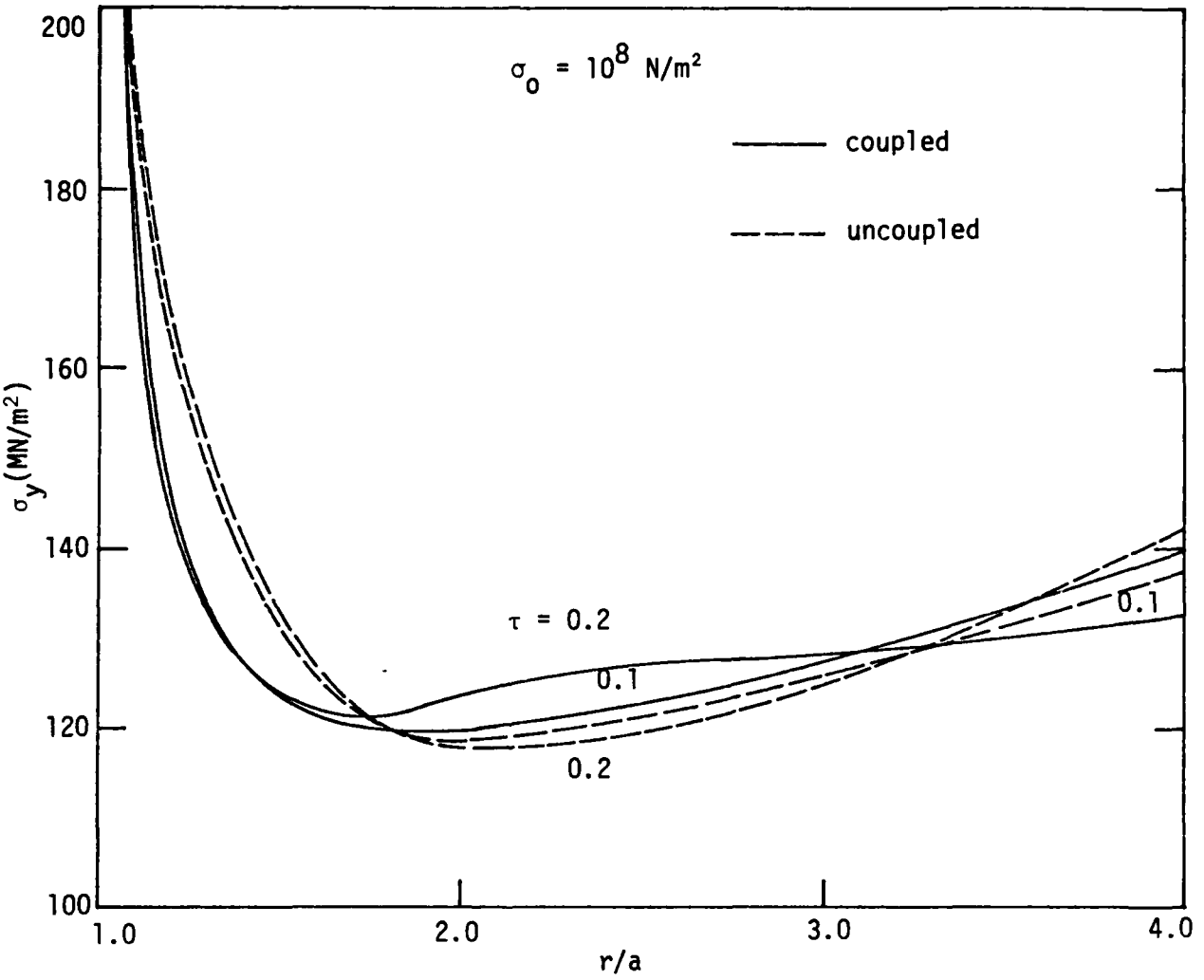

Figure 20 - Variation of stress σ_y versus distance along x axis for sudden temperature change on circular cavity. Material T300/5208 laminate

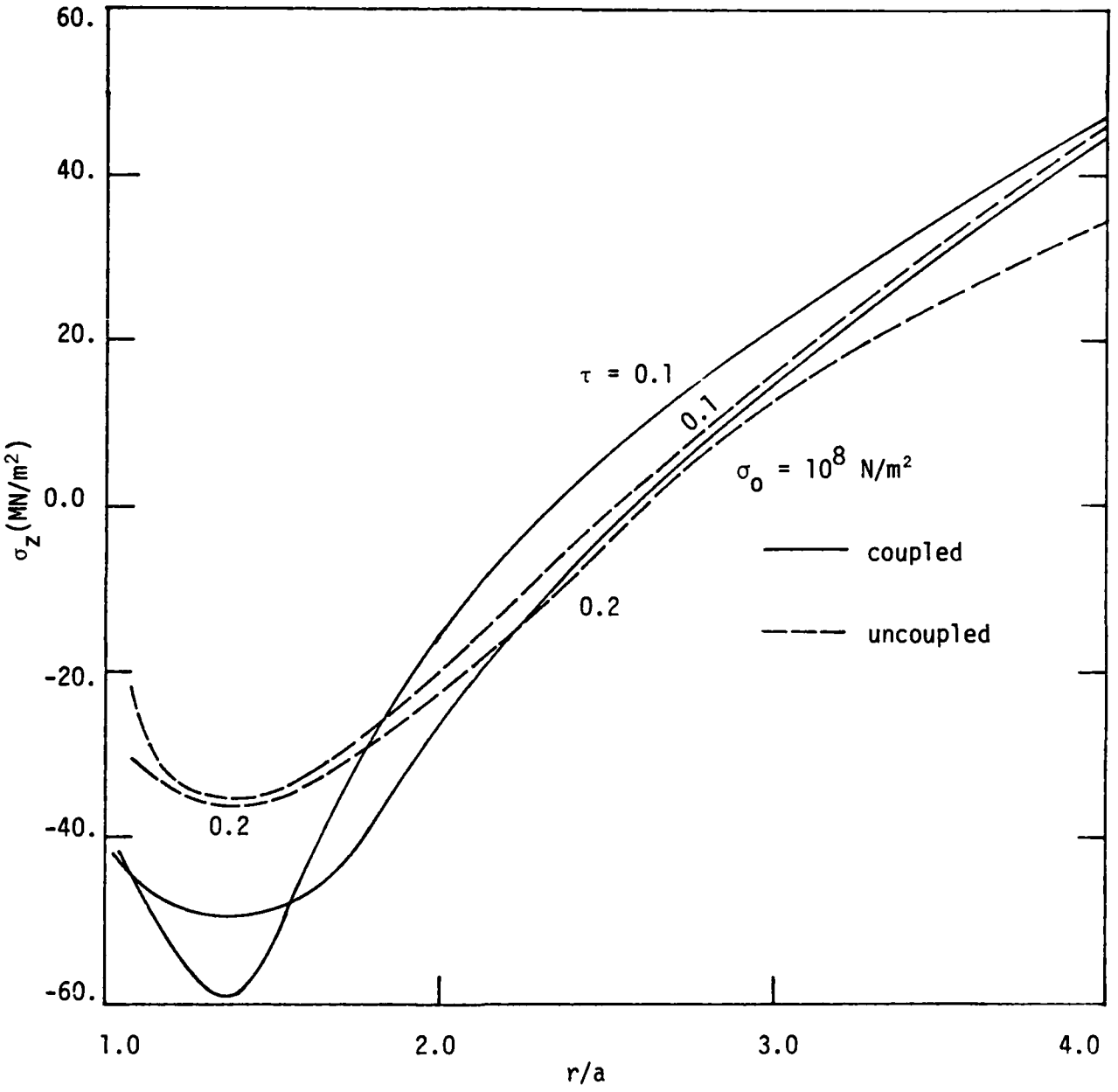

Figure 21 - Variation of stress σ_z versus distance along x axis for sudden temperature change on circular cavity. Material T300/5208 laminate

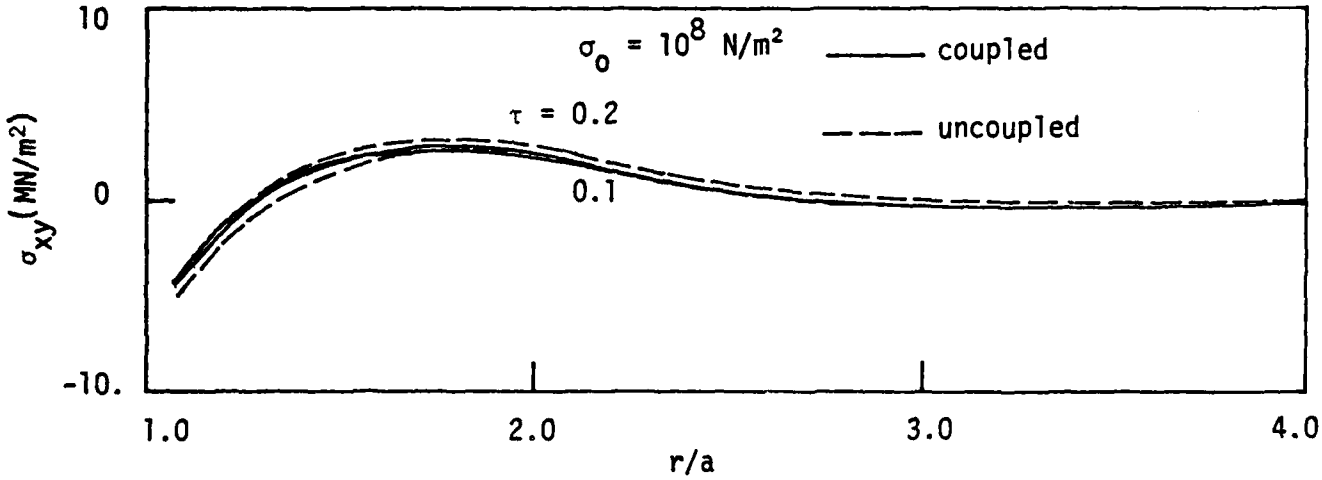

Figure 22 - Variation of stress σ_{xy} versus distance along x axis for sudden temperature change on circular cavity. Material T300/5208 laminates

$$\frac{dW}{dV} = \int_0^{\varepsilon_{ij}} \sigma_{ij} d\varepsilon_{ij} + f(\Delta T), \quad i,j = 1,2,3 \tag{69}$$

in which σ_{ij} and ε_{ij} are the rectangular components of the stress and strain tensor. The function $f(\Delta T)$ in equation (69) cannot be arbitrarily dropped for non-uniform states of temperature. It is given by

$$f(\Delta T) = \frac{3G}{1-2\nu_p} \alpha^2 (T-T_o)^2 \tag{70}$$

Although the function $f(\Delta T)$ does not affect the stress and strain state in the solid, it does influence the energy density state and hence the prediction of failure sites should dW/dV be used in the failure criterion.

The basic idea in the strain energy density criterion relies on the assumption that failure modes can be uniquely identified with threshold or critical values of dW/dV. The locations of yielding and fracture initiation are asso-

ciated, respectively, with the relative maximum and minimum values of dW/dV with reference to the space variables, say r and θ in polar coordinates for two-dimensional problems. The variations of dW/dV with θ or r determine the locations of $(dW/dV)_{max}$ and $(dW/dV)_{min}$. A critical value of dW/dV or $(dW/dV)_c$, which can be obtained from the area under the true stress-strain curve in a uniaxial tensile test at fracture, is assumed to govern the condition of fracture initiation, i.e., when $(dW/dV)_{min} = (dW/dV)_c$.

For a linear elastic, isotropic and homogeneous material, equation (69) can be written simply as

$$\frac{dW}{dV} = \frac{1+\nu_p}{2E}\left[\sigma_x^2 + \sigma_y^2 + \sigma_z^2 - \frac{\nu_p}{1+\nu_p}(\sigma_x + \sigma_y + \sigma_z)^2 + 2\sigma_{xy}^2\right] \tag{71}$$

provided that

$$f(\Delta T) = \frac{3G}{1-2\nu_p}(\alpha\Delta T)^2 \tag{72}$$

In addition, if the problem is in a state of plane strain, the additional condition

$$\sigma_z = \nu_p(\sigma_x+\sigma_y) - \alpha E\Delta T \tag{73}$$

must be imposed. Hence, dW/dV for the T300/5208 composite laminate can be computed without difficulty. Because of symmetry with respect to the x-axis, $(dW/dV)_{min}$ will occur at $\theta = 0$ and hence it is only necessary to differentiate (dW/dV) with reference to r for determining $(dW/dV)_{min}$.

Moisture Boundary Condition. Referring to the boundary conditions specified by equations (66) where the moisture on the hole is raised from 0% to 75% RH with the temperature held constant at 21°C, the variations of dW/dV with r/a for $\theta = 0$ are shown in Figure 23 for $\tau = 7.5$ and $\sigma_o = 5 \times 10^7$, 10^8 N/m^2. Indeed,

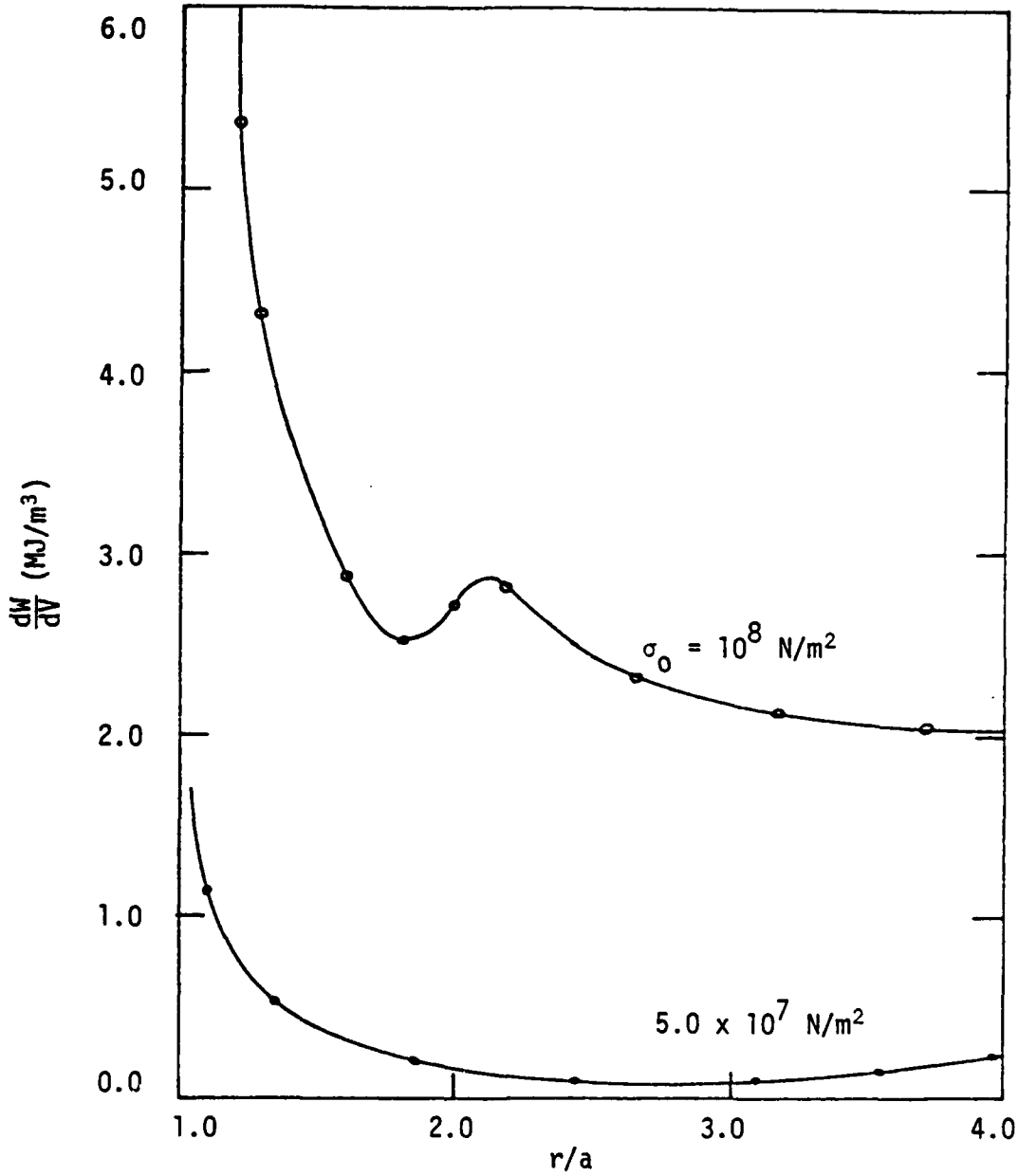

Figure 23 - Variations of strain energy density with distance for sudden moisture change in T300/5208 containing a circular cavity for $\tau = 7.5$

the solid curves possessed relative minima at r/a approximately equal to 2.975 for $\sigma_o = 5 \times 10^7$ N/m^2 and 1.850 for $\sigma_o = 10^8$ N/m^2. Increase in the magnitude of

the applied stress σ_o tends to shift the location of $(dW/dV)_{min}$ closer to the hole boundary. Figure 24 gives a plot of the minima of dW/dV against the dimensionless time parameter τ. For $\sigma_o = 5.0 \times 10^7$ N/m^2, $(dW/dV)_{min}$ rises sharply at

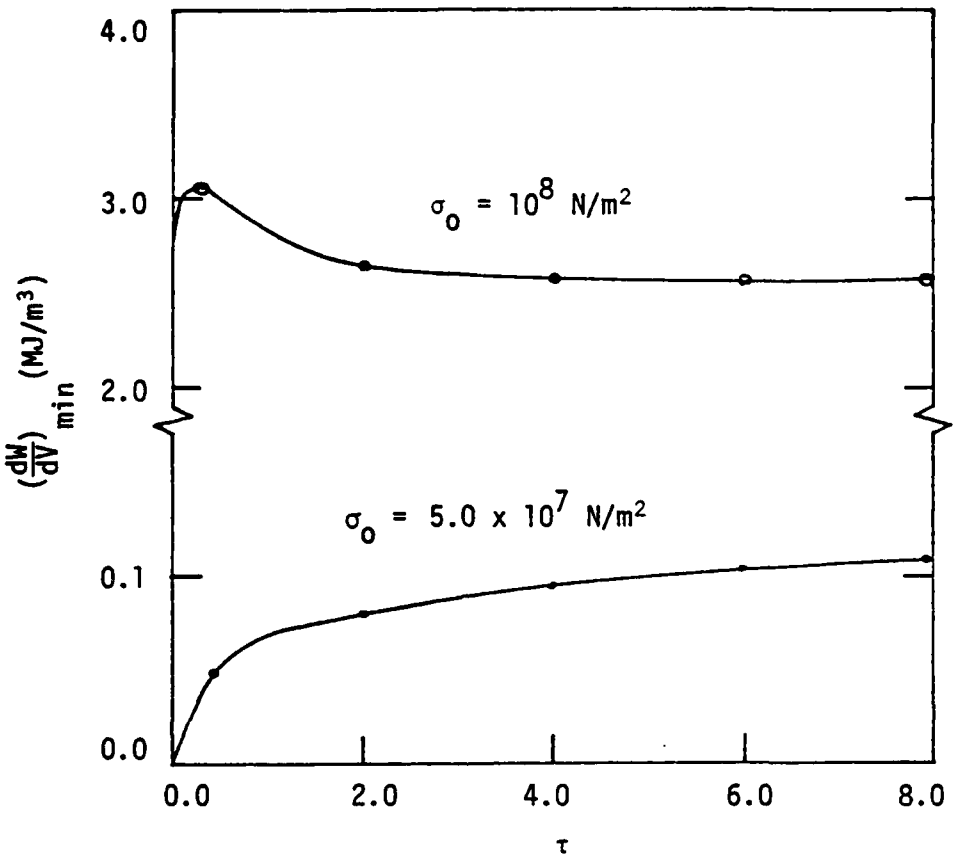

Figure 24 - Variations of minimum strain energy with τ for sudden moisture change in T300/5208 containing a circular cavity

first and then levels off. The time at which failure occurs depends on the intersection of the $(dW/dV)_c$ line with the $(dW/dV)_{min}$ curve. The opposite trend is observed when σ_o is increased to 10^8 N/m^2 where $(dW/dV)_{min}$ rised slightly at first and then decayed monotonically. When the deformation is decoupled from diffusion, the amplitude of $(dW/dV)_{min}$ decreases appreciably as the dotted curve in Figure 25 for $\sigma_o = 5.0 \times 10^7$ N/m^2 is seen to lie below the solid curve.

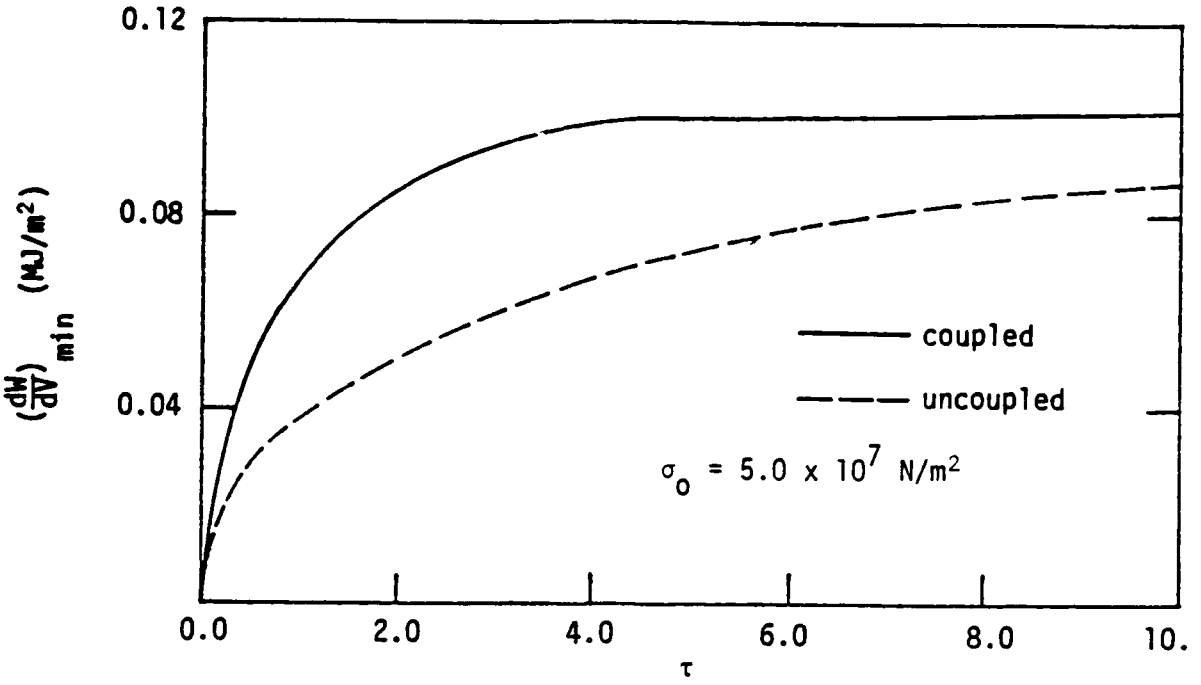

Figure 25 - Minimum strain energy density as a function of time for sudden moisture change on circular cavity. Material T300/5208 laminates

Temperature Boundary Condition. The boundary conditions corresponding to sudden temperature rise are given in equations (68). A 40°C of temperature increase from 21°C to 61°C is applied to the hole while keeping the moisture constant at 75% RH. The numerical results are displayed graphically in Figures 26 and 27 for $\sigma_o = 10^8$ N/m . The general trend of dW/dV decaying with r/a is seen in Figure 26 for $\tau = 0.2$. A relatively weak minimum of dW/dV is detected at r/a ≈ 2.80 and the difference between stress coupling and uncoupling is small. Figure 27 gives a plot of $(dW/dV)_{min}$ versus the dimensionless time parameter τ. Aside from the difference in magnitude of $(dW/dV)_{min}$ between the solid and dotted curve, their trend is opposite. The coupled theory yields values of $(dW/dV)_{min}$ increase with time while the uncoupled theory predicts the opposite. Stress coupling effect is thus seen to be significant both quantitatively and qualitatively.

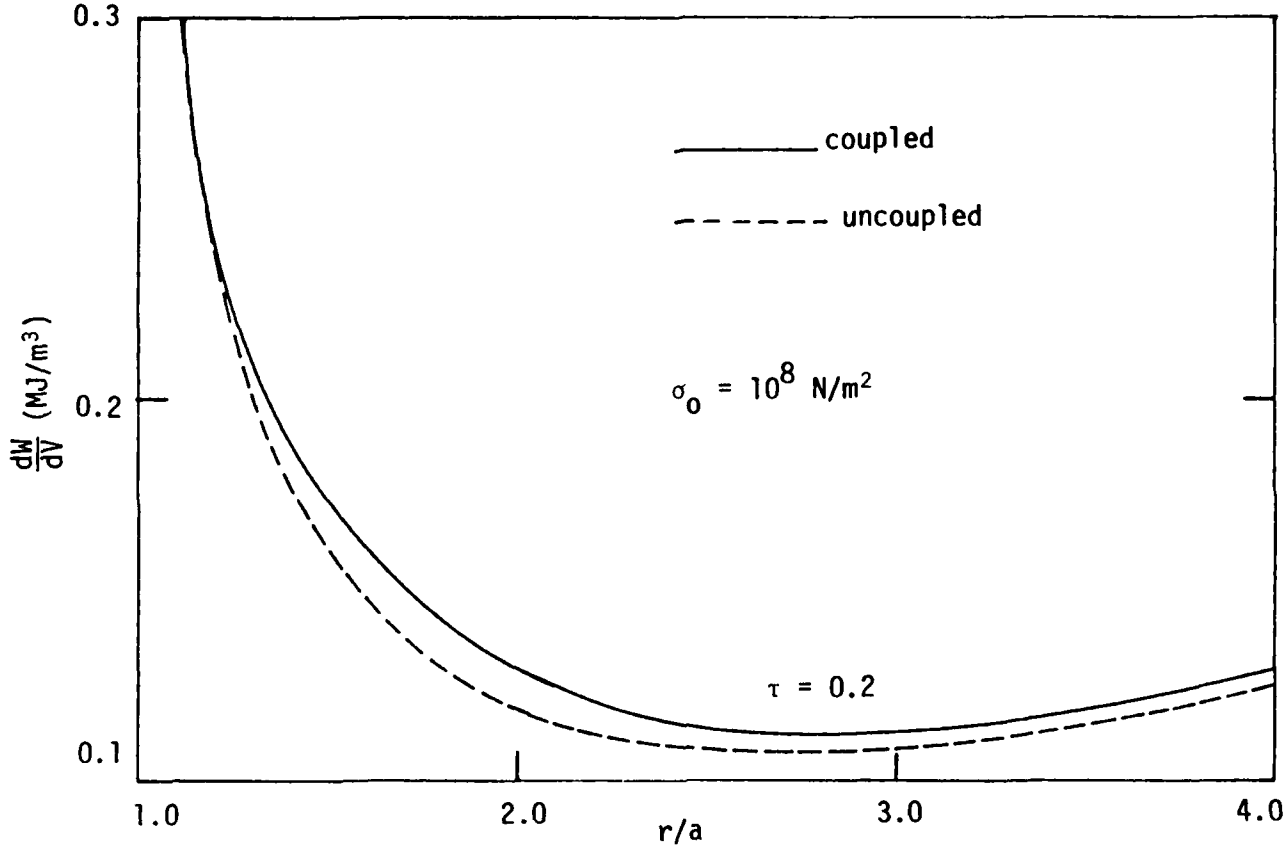

Figure 26 - Variations of strain energy density with distance for sudden temperature change in T300/5208 laminate having a circular cavity

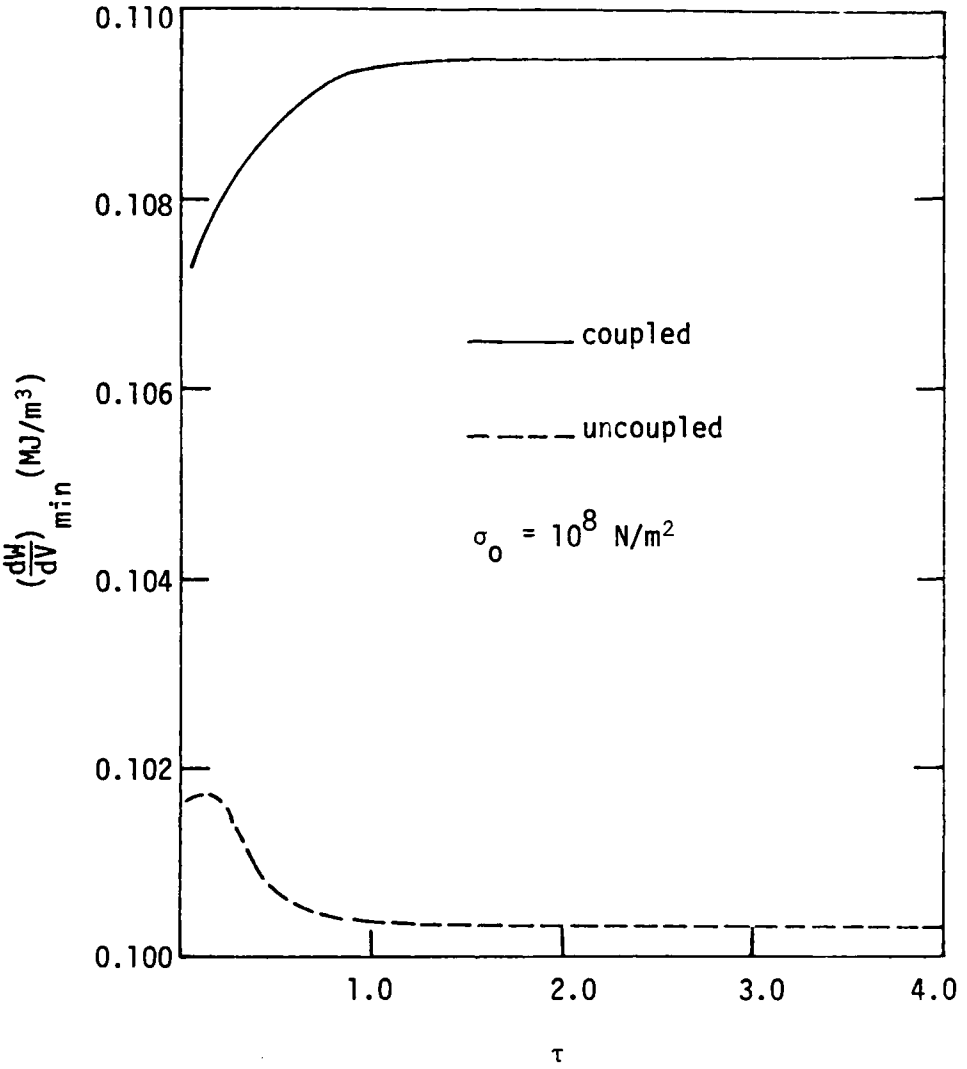

Figure 27 - Variations of minimum strain energy with τ for sudden temperature change in T300/5208 laminate having a circular cavity

CONCLUDING REMARKS

The major contribution of this work may not lie in the formulation of a hygrothermal elasticity theory which considers coupling between mechanical deformation and diffusion but the *analytical scheme* for evaluating the physical constants that allowed a numerical evaluation of the results. In consistent with the re-

cent experimental observations [5], the applied mechanical stresses can strongly influence the moisture distribution within composite materials. Such observation obviously suggests a strong interaction between the deformation and moisture diffusion process. The predictions made on the T300/5208 composite laminate with a circular cavity show that stress coupling can influence the results both quantitatively and qualitatively by a wide margin. The neglect of stress coupling leads to unconservative predictions for the transient moisture and temperature boundary considered in this investigation. Such findings, however, may not be valid in general as coupling effects are sensitive to changes in the combination of moisture, temperature and stress boundary conditions. The influence of stress coupling is *case-specific* and should be investigated by analyses and/or experiments to determine the extent of its influence.

The present work should be regarded only as a preliminary effort towards the development of a fundamental basis for understanding the continuum parameters that control material damage in the presence of moisture and temperature in addition to mechanical stresses. Moisture enhanced crack growth in a stressed environment is one of the least understood phenomena in fracture mechanics. There is no doubt that diffusion and mechanical deformation in front of a sharp crack undergo strong interaction. Such studies are presently being carried out in the Institute of Fracture and Solid Mechanics at Lehigh and should lead to a better understanding of material damage enhanced by moisture and temperature.

REFERENCES

[1] G. C. Sih and M. T. Shih, "Hygrothermal Stress in a Plate Subjected to Antisymmetric Time-Dependent Moisture and Temperature Boundary Conditions", J. Thermal Stresses, Vol. 3, pp. 321-340, 1980.

[2] R. J. Hartranft and G. C. Sih, "The Influence of the Soret and Dufour Effects on the Diffusion of Heat and Moisture in Solids", Mekhanika Kompozitnykh Materialov, No. 1, pp. 53-61, January-February, 1980.

[3] G. C. Sih, M. T. Shih and S. C. Chou, "Transient Hygrothermal Stresses in Composites: Coupling of Moisture and Heat with Temperature Varying Diffusivity", Int. J. Engng. Sci., Vol. 18, pp. 19-42, 1980.

[4] R. J. Hartranft, G. C. Sih and T. S. Chen, "Interaction of Temperature and Moisture in Diffusion", Technical Report AFOSR-TR-77-1, Bolling Air Force Base, D.C., 1977.

[5] G. Marom and L. J. Broutman, "Moisture Penetration into Composites under External Stress", Polymer Composites, Vol. 2, No. 3, pp. 132-136, 1981.

[6] G. C. Sih, "A Special Theory of Crack Propagation: Methods of Analysis and Solutions of Crack Problems", Mechanics of Fracture I, edited by G. C. Sih, Noordhoff International Publishing, Leyden, pp. 21-45, 1973.

[7] G. C. Sih, "A Three-Dimensional Strain Energy Density Factor Theory of Crack Propagation: Three Dimensional Crack Problems", Mechanics of Fracture II, edited by G. C. Sih, Noordhoff International Publishing, Leyden, pp. 15-53, 1975.

[8] Ya. S. Podstrigach and V. S. Pavlina, "Fundamental Equations of Plane Thermodiffusion Problems", Priki. Mekh., 1, No. 3, pp. 101-106, 1965.

[9] H. N. Friedlander and J. D. Calfee, "The Importance of Fabrication Technology in Translation of Fiber and Matrix Properties to Advanced Composites", Polyblends and Composites, Paul F. Bruins, ed., Interscience Publishers, 1970.

[10] J. D. Thomas, "Effect of Inorganic Fillers on Coefficient of Thermal Expansion of Polymeric Materials", AD 287, 826, 24 pp., 1960.

[11] T. T. Wang and K. T. Kwei, "Effect of Induced Thermal Stresses on the Coefficients of Thermal Expansion and Densities of Filled Polymers", J. Polym. Sci., A-2, Vol. 7, pp. 889-896, 1969.

[12] S. W. Tsai, J. C. Halpin and N. J. Pagano, Composite Materials Workshop, Technomic, Stamford, Conn., pp. 233-253, 1968.

[13] D. F. Adams and A. K. Miller, "The Influence of Material Variability on the Predicted Environmental Behavior of Composite Materials", J. Engng. Materials and Technology, Vol. 100, pp. 77-83, January 1978.

[14] Shirrell, C. D., "Moisture Diffusion in Advanced Composite Resin Matrix Laminates", AFML Progress Report, Bergamo Center, 1977.

[15] G. C. Sih and A. Ogawa, "Transient Hygrothermal and Mechanical Stress Intensities Around Cracks", Fracture of Composite Materials, edited by G. C. Sih and V. P. Tamuzs, Martinus Nijhoff Publishers, The Hague, pp. 79-90, 1982.

[16] S. C. Chou, G. C. Sih and M. T. Shih, "Moisture and Temperature Effects on the Transient Stresses Around Crack-Like Defects", Presented at International Conference on Application of Fracture Mechanics to Materials and Structures, Freiburg, Germany, June 20-24, 1983.

DISTRIBUTION LIST

	No. of Copies
Office of Deputy Under Secretary of Defense for Research and Engineering (ET) ATTN: Mr. J. Persh, Staff Specialist for Materials and Structures (Room 3D1089) The Pentagon Washington, DC 20301	1
Office of Deputy Chief of Research Development and Acquisition ATTN: DAMA-CSS/Dr. J. I. Bryant (Room 3D424) The Pentagon Washington, DC 20301	1
Commander U.S. Army Materiel Development and Readiness Command ATTN: DRCLDC, R. Gonano, Office of Laboratory Management 5000 Eisenhower Avenue Alexandria, VA 22333	1
Director Ballistic Missile Defense Systems Command ATTN: BMDSC-TEN, Mr. N. J. Hurst	1
BMDSC-LEI, Mr. J. Katechis	1
BMDSC-LEI, Mrs. R. Buckelew	1
BMDSC-AOLIB P.O. Box 1500 Huntsville, AL 35807	1
Ballistic Missile Defense Program Office ATTN: DACS-BMT DARCOM Bldg., Seventh Floor 5001 Eisenhower Avenue Alexandria, VA 22333	1
Director Ballistic Missile Defense Advanced Technology Center ATTN: ATC-X, Dr. J. Carlson	1
ATC-X, Col. F. Gray	1
ATC-R, D. Russ	1
ATC-R, Maj. J. Hovious	1
ATC-R, M. Whitfield	1
ATC-M, D. Harmon	1
ATC-M, J. Papadopoulos P.O. Box 1500 Huntsville, AL 35807	1

	No. of Copies
Director Defense Nuclear Agency ATTN: SPAS, Dr. J. Slaughter Washington, DC 20305	1
Director Army Ballistic Research Laboratories ATTN: DRDAR-BLT, Dr. N. J. Huffington, Jr. DRDAR-BLT, Dr. T. W. Wright DRDAR-BLT, Dr. G. L. Moss Aberdeen Proving Ground, MD 21005	 1 1 1
Commander Harry Diamond Laboratories ATTN: DRXDO-NP, Dr. F. Wimenitz 2800 Powder Mill Road Adelphi, MD 20783	1
Commander Air Force Materials Laboratory Air Force Systems Command ATTN: LNE/Dr. W. Kessler LNC/Dr. D. Schmidt Wright-Patterson Air Force Base Dayton, OH 45433	 1 1
Commander BMO/ABRES Office ATTN: BMO/MNRT, Col. R. Smith BMO/MNRTE, Maj. J. Sikra BMO/MNRTE, Maj. K. Yelmgren Norton Air Force Base, CA 92409	 1 1 1
Commander Air Force Materials Laboratory ATTN: AFML/MBM, Dr. S. W. Tsai Wright-Patterson Air Force Base Dayton, OH 45433	 1
Commander Naval Ordnance Systems Command ATTN: ORD-03331, Mr. M. Kinna Washington, DC 20360	 1

	No. of Copies
Commander Naval Surface Weapons Center ATTN: Dr. C. Lyons Dr. W. Messick Silver Springs, MD 20910	 1 1
Lawrence Livermore National Laboratory ATTN: Dr. E. M. Wu P.O. Box 808 (L-342) Livermore, CA 94550	 1
Sandia Laboratories ATTN: Dr. Frank P. Gerstle, Jr. Dr. L. D. Bertholf Dr. J. Lipkin P.O. Box 5800 Albuquerque, NM 87115	 1 1 1
Aerospace Corporation ATTN: Dr. R. Cooper P.O. Box 92975 Los Angeles, CA 90009	 1
AVCO Corporation Government Products Group ATTN: Dr. W. Reinecke Mr. P. Rolincik 201 Lowell Street Wilmington, MA 01997	 1 1
Boeing Commercial Airplane Company ATTN: Dr. K. Y. Lin Mail Stop 6W-13 Seattle, WA 98124	 1
ETA Corporation ATTN: D. L. Mykkanen P.O. Box 6625 Orange, CA 92667	 1
Effects Technology, Inc. ATTN: Dr. R. Wengler Dr. R. Parisse J. Green 5383 Hollister Avenue Santa Barbara, CA 93111	 1 1 1

	No. of Copies
Fiber Materials, Inc.	
ATTN: M. Subilia, Jr.	1
L. Landers	1
R. Burns	1
Biddeford Industrial Park	
Biddeford, ME 04005	
General Electric Company	
Advanced Materials Development Laboratory	
ATTN: Ms. B. Maguire, Room 5400B	1
L. Pochettino, Room 5300B	1
K. Hall, Room 5700	1
J. Brazel, Room 5411B	1
D. Stewart, Room 5211	1
3198 Chestnut Street	
Philadelphia, PA 19101	
General Dynamics Corporation	
Convair Division	
ATTN: J. Hertz	1
H. McCutcheon, Jr.	1
5001 Kearny Villa Road	
San Diego, CA 92138	
General Dynamics Corporation	
ATTN: Dr. D. J. Wilkins, Mail Zone 2884	1
P.O. Box 748	
Fort Worth, TX 76101	
Kaman Sciences Corporation	
ATTN: D. Williams	1
P.O. Box 7463	
Colorado Springs, CO 80933	
Ktech	
ATTN: Dr. D. Keller	1
911 Pennsylvania Avenue, N.E.	
Albuquerque, NM 87110	
Lehigh University	
Institute of Fracture and Solid Mechanics	
ATTN: Dr. George C. Sih	1
Bldg. 19, Packard Lab	
Bethlehem, PA 18015	
Lockheed Missiles and Space Company	
ATTN: D. Aspinwall	1
P.O. Box 504	
Sunnyvale, CA 94088	

	No. of Copies
Lehigh University Institute of Fracture and Solid Mechanics ATTN: Dr. George C. Sih Bldg. 19, Packard Lab Bethlehem, PA 18015	1
Lockheed Missiles and Space Company ATTN: Mr. D. Aspinwall P.O. Box 504 Sunnyvale, CA 94088	1
Martin Marietta Aerospace ATTN: Mr. V. Hewitt Mr. Frank H. Koo P.O. Box 5837 Orlando, FL 32805	1 1
Massachusetts Institute of Technology Department of Aeronautics and Astronautics ATTN: Professor Theodore H. Pian Professor James Mar 77 Mass Avenue Cambridge, MA 02139	1 1
McDonnell Douglas Corporation ATTN: Dr. L. Cohen Mr. H. Parachanian 5301 Bolsa Avenue Huntington Beach, CA 92647	1 1
Pacifica Technology, Inc. ATTN: Dr. Ponsford P.O. Box 148 Del Mar, CA 92014	1
Prototype Development Associates, Inc. ATTN: Mr. J. Schultzler Mr. N. Harrington 1740 Garry Avenue, Suite 201 Santa Ana, CA 92705	1 1
Radkowski Associates ATTN: Dr. P. Radkowski P.O. Box 5474 Riverside, CA 92507	1

	No. of Copies
Rensselaer Polytechnic Institute Department of Applied Mechanics ATTN: Professor E. H. Lee Troy, NY 12181	1
Southwest Research Institute ATTN: A. Wenzel 8500 Culebra Road San Antonio, TX 78206	1
Terra Tek, Inc. ATTN: Dr. A. H. Jones 420 Wakara Way Salt Lake City, UT 84108	1
University of Illinois at Chicago Department of Materials Engineering ATTN: Professor R. L. Spilker Chicago, IL 60680	1
Defense Documentation Center Cameron Station, Bldg. 5 5010 Duke Station Alexandria, VA 22314	1
Director Army Materials and Mechanics Research Center ATTN: DRXMR-B, J. F. Dignam	1
DRXMR-B, Dr. S. C. Chou	10
DRXMR-B, L. R. Aronin	1
DRXMR-B, Dr. D. P. Dandekar	1
DRXMR-K, Procurement Office	1
DRXMR-PL, Library	2
DRXMR-PR, Technical Reports Office Watertown, MA 02172	1

Army Materials and Mechanics Research Center
Watertown, Massachusetts 02172
SULFIDE INCLUSIONS IN ELECTROSLAG
REMELTED STEELS
M. D. Boldy, T. Fujii, D. R. Poirier
M. C. Flemings
Massachusetts Institute of Technology
Cambridge, MA 02139
Final Technical Report AMMRC-81-4, January 1981, 122 pp
illus.-tables, Contract DAAG46-78-C-0032
D/A Project: 1L161102AH42: AMCMS Code, 61102A
Final Report, December 1977 to December 1979

AD ______________
Unclassified
Unlimited Distribution

Key Words
Precipitation
Electroslag refining
Alloy steels

The relationships among heat treatment, sulfide inclusion distribution and chemistry were investigated in this work, and the problem of overheating found to be directly related to these parameters. A basis for comparison was found in microscopic examination of carbon extraction replicas from commercially produced electroslag remelted steel. This showed a direct correlation between sulfide inclusion distribution and overheating. Further investigation characterized a critical cooling rate necessary for overheating to occur. Methods for eliminating the problem of sulfide inclusions in ESR steels were examined in detail. The simplest is to alter the cooling rate through the overheating range. Either a fast or a very slow cool eliminates the problem. An alternate method of eliminating the problem is to change the chemistry of the steel. These different techniques were examined in this work. All three were tested and proved to be successful in eliminating the sulfide problem. In an associated study a model to simulate the diffusion controlled coarsening and dissolution kinetics of particles. Within a metallic matrix was formulated. Calculations were made and compared with experiments in a model system and on manganese sulfide inclusions in iron. The effect of the manganese and sulfur content was studied. Agreement of the calculations is good.

Army Materials and Mechanics Research Center
Watertown, Massachusetts 02172
SULFIDE INCLUSIONS IN ELECTROSLAG
REMELTED STEELS
M. D. Boldy, T. Fujii, D. R. Poirier
M. C. Flemings
Massachusetts Institute of Technology
Cambridge, MA 02139
Final Technical Report AMMRC-81-4, January 1981, 122 pp
illus.-tables, Contract DAAG46-78-C-0032
D/A Project: 1L161102AH42: AMCMS Code, 61102A
Final Report, December 1977 to December 1979

AD ______________
Unclassified
Unlimited Distribution

Key Words
Precipitation
Electroslag refining
Alloy steels

The relationships among heat treatment, sulfide inclusion distribution and chemistry were investigated in this work, and the problem of overheating found to be directly related to these parameters. A basis for comparison was found in microscopic examination of carbon extraction replicas from commercially produced electroslag remelted steel. This showed a direct correlation between sulfide inclusion distribution and overheating. Further investigation characterized a critical cooling rate necessary for overheating to occur. Methods for eliminating the problem of sulfide inclusions in ESR steels were examined in detail. The simplest is to alter the cooling rate through the overheating range. Either a fast or a very slow cool eliminates the problem. An alternate method of eliminating the problem is to change the chemistry of the steel. These different techniques were examined in this work. All three were tested and proved to be successful in eliminating the sulfide problem. In an associated study a model to simulate the diffusion controlled coarsening and dissolution kinetics of particles. Within a metallic matrix was formulated. Calculations were made and compared with experiments in a model system and on manganese sulfide inclusions in iron. The effect of the manganese and sulfur content was studied. Agreement of the calculations is good.

Army Materials and Mechanics Research Center
Watertown, Massachusetts 02172
SULFIDE INCLUSIONS IN ELECTROSLAG
REMELTED STEELS
M. D. Boldy, T. Fujii, D. R. Poirier
M. C. Flemings
Massachusetts Institute of Technology
Cambridge, MA 02139
Final Technical Report AMMRC-81-4, January 1981, 122 pp
illus.-tables, Contract DAAG46-78-C-0032
D/A Project: 1L161102AH42: AMCMS Code, 61102A
Final Report, December 1977 to December 1979

AD ______________
Unclassified
Unlimited Distribution

Key Words
Precipitation
Electroslag refining
Alloy steels

The relationships among heat treatment, sulfide inclusion distribution and chemistry were investigated in this work, and the problem of overheating found to be directly related to these parameters. A basis for comparison was found in microscopic examination of carbon extraction replicas from commercially produced electroslag remelted steel. This showed a direct correlation between sulfide inclusion distribution and overheating. Further investigation characterized a critical cooling rate necessary for overheating to occur. Methods for eliminating the problem of sulfide inclusions in ESR steels were examined in detail. The simplest is to alter the cooling rate through the overheating range. Either a fast or a very slow cool eliminates the problem. An alternate method of eliminating the problem is to change the chemistry of the steel. These different techniques were examined in this work. All three were tested and proved to be successful in eliminating the sulfide problem. In an associated study a model to simulate the diffusion controlled coarsening and dissolution kinetics of particles. Within a metallic matrix was formulated. Calculations were made and compared with experiments in a model system and on manganese sulfide inclusions in iron. The effect of the manganese and sulfur content was studied. Agreement of the calculations is good.

Army Materials and Mechanics Research Center
Watertown, Massachusetts 02172
SULFIDE INCLUSIONS IN ELECTROSLAG
REMELTED STEELS
M. D. Boldy, T. Fujii, D. R. Poirier
M. C. Flemings
Massachusetts Institute of Technology
Cambridge, MA 02139
Final Technical Report AMMRC-81-4, January 1981, 122 pp
illus.-tables, Contract DAAG46-78-C-0032
D/A Project: 1L161102AH42: AMCMS Code, 61102A
Final Report, December 1977 to December 1979

AD ______________
Unclassified
Unlimited Distribution

Key Words
Precipitation
Electroslag refining
Alloy steels

The relationships among heat treatment, sulfide inclusion distribution and chemistry were investigated in this work, and the problem of overheating found to be directly related to these parameters. A basis for comparison was found in microscopic examination of carbon extraction replicas from commercially produced electroslag remelted steel. This showed a direct correlation between sulfide inclusion distribution and overheating. Further investigation characterized a critical cooling rate necessary for overheating to occur. Methods for eliminating the problem of sulfide inclusions in ESR steels were examined in detail. The simplest is to alter the cooling rate through the overheating range. Either a fast or a very slow cool eliminates the problem. An alternate method of eliminating the problem is to change the chemistry of the steel. These different techniques were examined in this work. All three were tested and proved to be successful in eliminating the sulfide problem. In an associated study a model to simulate the diffusion controlled coarsening and dissolution kinetics of particles. Within a metallic matrix was formulated. Calculations were made and compared with experiments in a model system and on manganese sulfide inclusions in iron. The effect of the manganese and sulfur content was studied. Agreement of the calculations is good.

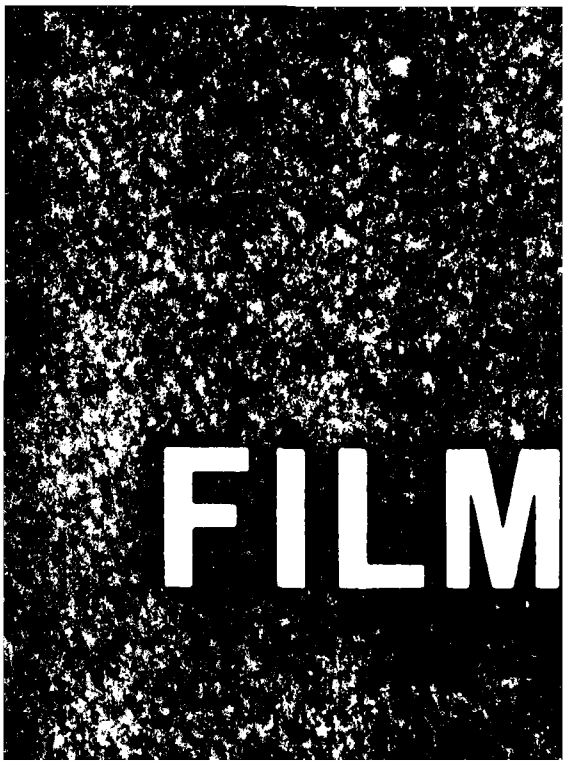
FILM